nature photonics

LETTERS

https://doi.org/10.1038/s41566-018-0213-5

A phonon laser operating at an exceptional point

Jing Zhang[1,2,3,10], Bo Peng[1,8,10], Şahin Kaya Özdemir[1,9], Kevin Pichler[4], Dmitry O. Krimer[4], Guangming Zhao[1], Franco Nori[5,6], Yu-xi Liu[3,7], Stefan Rotter[4] and Lan Yang[1*]

Non-Hermitian physical systems have attracted considerable attention lately for their unconventional behaviour around exceptional points (EPs)—spectral singularities at which eigenvalues and eigenvectors coalesce. In particular, many new EP-related concepts such as unidirectional lasing and invisibility, as well as chiral transmission, have been realized. Given the progress in understanding the physics of EPs in various photonic structures, it is surprising that one of the oldest theoretical predictions associated with them, a remarkable broadening of the laser linewidth at an EP, has been probed only indirectly so far. Here, we fill this gap by steering a phonon laser through an EP in a compound optomechanical system formed by two coupled resonators. We observe a pronounced linewidth broadening of the mechanical lasing mode generated in one of the resonators when the system approaches the EP.

Non-Hermitian systems featuring EPs have attracted attention in many fields of physics[1,2]. In particular, there has been an increasing number of experiments in recent years that have not only demonstrated unique properties of EPs, such as the topology of self-intersecting Riemann sheets around them[3,4], but also led to proposals of practical applications based on features associated with EPs, such as loss-induced transmission and unidirectional invisibility[5–11], chiral behaviour[12], mode selection in lasers[13–15], enhanced sensors[16–19] and topological energy transfer[3,20]. A special share of attention has been dedicated to EPs in parity–time symmetric systems, where resonant or guided modes can be efficiently controlled by sweeping them across an EP[5–7].

Historically, one of the first predictions associated with EPs is the extreme broadening of the laser linewidth[21,22] beyond the fundamental Schawlow–Townes limit[23]. This broadening is quantified by the Petermann factor[24,25], which measures the excess quantum noise induced by the non-orthogonality of resonator modes. Specifically, the coupling between modes, induced by the openness of the resonator and the internal dissipation, is translated into excess noise by the gain mechanism and the cavity feedback[26]. Although early work showed that this linewidth broadening due to non-orthogonal resonator modes can, indeed, be measured[27–29], only subsequent theoretical work associated a pronounced linewidth enhancement in unstable laser resonators with the presence of a nearby EP[22]. What really happens to the linewidth when a laser operates at an EP has remained unclear to this day. Standard laser theory[24,25] and general arguments based on self-orthogonality of modes[2] predict an unphysical divergence of the laser linewidth at the EP[21,30,31] where modes coalesce and become completely non-orthogonal (that is, parallel). More recent theoretical models provide a more consistent framework for calculating the laser linewidth[32–35] but fail to resolve the problems directly at the EP. Experimentally, it is not straightforward to steer a laser directly to an EP[13,36,37] nor to measure its extremely narrow linewidth. Additionally, laser modes have a tendency to become unstable close to an EP where the spectral vicinity of a second mode may lead to chaotic lasing that could be wrongly perceived as an extremely broad laser line.

Here, we provide a new strategy to tackle this problem by working with a phonon laser rather than with its optical counterpart. Phonon lasers that produce coherent sound oscillations (mechanical vibrations) induced by optical pumping have been introduced recently[38], and have been studied theoretically within the framework of parity–time symmetry and EP physics with many interesting predictions, such as thresholdless phonon lasing[39]. For a study of lasing at an EP, phonon lasers have the crucial advantage that the linewidth measurement is much easier than for an optical laser. Moreover, as we will discuss below, the phonon laser considered in this study provides an interesting platform to study EPs in atomic spectra[40].

The concept of the phonon laser used here is based on a system developed by Grudinin, Vahala and co-workers[38], who showed that a system of two coupled optical microresonators, one of which supports a mechanical mode, can produce coherent mechanical oscillations with characteristics that are typical for photon lasers, such as a threshold, a linewidth narrowing above threshold, and nonlinear saturation effects. To drive the mechanical mode resonantly, the frequency difference of the two optical supermodes formed through inter-resonator coupling is matched with the frequency of the mechanical mode. In analogy to a photon laser, here the two optical supermodes correspond to the ground and excited states of an atomic two-level system, and the mechanical mode (phonons) mediates the transition between them. The energy difference between the optical supermodes can be finely tuned, either by changing the distance between the resonators or by introducing additional loss to the resonator without the mechanical mode, such that the spectrum exhibits an EP. Therefore, this configuration provides an interesting platform on which to study not only lasing at an EP but also EPs in atomic spectra[40] (the two-level system here). In this sense, phonon lasing in this tunable 'two-level system' also brings in new conceptual aspects as compared with recent studies of EPs in photonic lasers in which EPs emerged owing to the overlapping of cavity modes while the energy levels of the gain material were kept fixed (here these roles are exchanged).

Our experimental platform is a compound optomechanical system composed of two coupled silica whispering-gallery-mode

[1]Department of Electrical and Systems Engineering, Washington University, St Louis, MO, USA. [2]Department of Automation, Tsinghua University, Beijing, China. [3]Center for Quantum Information Science and Technology, BNRist, Beijing, China. [4]Institute for Theoretical Physics, Vienna University of Technology (TU Wien), Vienna, Austria. [5]Theoretical Quantum Physics Laboratory, RIKEN, Saitama, Japan. [6]Physics Department, The University of Michigan, Ann Arbor, MI, USA. [7]Institute of Microelectronics, Tsinghua University, Beijing, China. [8]Present address: IBM Thomas J. Watson Research Center, Yorktown Heights, NY, USA. [9]Present address: Department of Engineering Science and Mechanics, The Pennsylvania State University, University Park, PA, USA. [10]These authors contributed equally: Jing Zhang, Bo Peng. *e-mail: yang@seas.wustl.edu

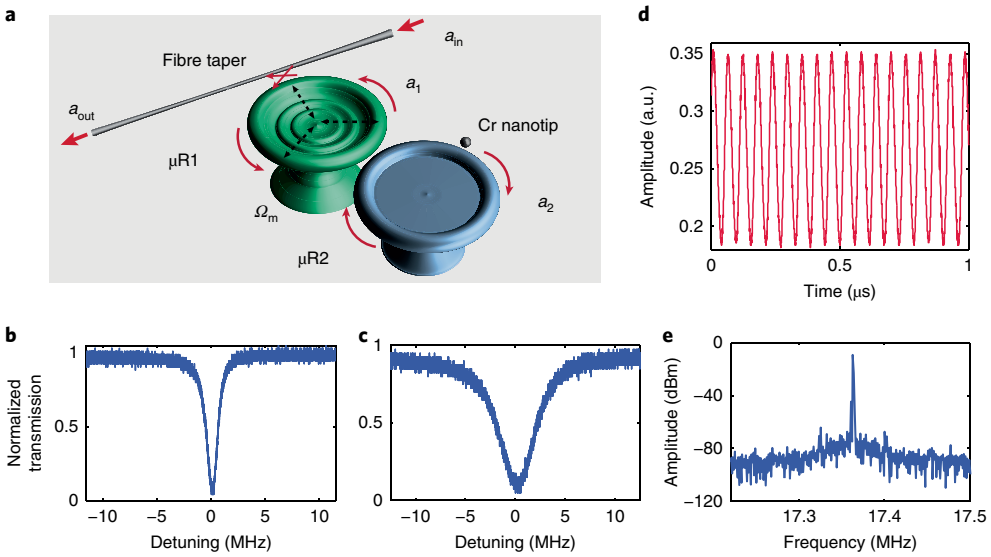

Fig. 1 | Phonon lasing in a compound resonator system. a, Schematic diagram of the compound phonon-laser system. Two microtoroid resonators, μR1 and μR2, are coupled to each other by evanescent fields. The first resonator μR1 supports a high-*Q* optical mode a_1 and a mechanical mode with resonance frequency Ω_m. The second resonator μR2 supports a low-*Q* optical mode a_2, and the damping rate of this low-*Q* mode can be tuned by a chromium-coated silica nanotip approaching μR2. **b**,**c**, Transmission spectra of the high-*Q* optical mode a_1 (**b**) and the low-*Q* optical mode a_2 (**c**) that exhibit Lorentzian lineshapes. **d**, Periodic time evolution of the mechanical mode supported by the resonator μR1. **e**, Radiofrequency spectrum of the mechanical mode in the phonon lasing regime.

microresonators (Fig. 1a) μR1 and μR2, where only the resonator μR1 supports a mechanical mode with frequency $\Omega_m = 17.38$ MHz and mechanical damping rate $\Gamma_m = 40$ kHz (measured just below the oscillation threshold). To optically excite the mechanical mode for phonon lasing, as well as to characterize the optical and mechanical modes, light from a tunable laser was coupled into μR1 by means of a tapered fibre, which was also used to out-couple the light from μR1 and direct it to a detector. The quality factors (Q) of the optical modes of μR1 and μR2 were 6.33×10^7 and 1.5×10^7, respectively. Typical transmission spectra obtained when the resonators were probed individually are given in Fig. 1b,c.

To steer the system towards or away from its EP, and to observe the behaviour of phonon lasing in the vicinity of an EP, we introduced additional loss to μR2 using a chromium-coated silica nanofibre tip (Fig. 1a), which has strong absorption in the 1,550-nm band. This additional loss, characterized by the damping rate γ_{tip}, was adjusted by increasing the overlap of the nanotip with the evanescent field of μR2. By introducing this extra loss for the optical modes, we tune the decay rates of the optical supermodes as well as their frequency difference, which then affect the interaction between the mechanical sound wave and this 'two-level system'. We used the thermo-optic effect to tune the resonance frequencies of the resonators to be the same before they were coupled. The inter-resonator distance was finely adjusted to control the coupling strength between the resonators, which induced the formation of two supermodes, and enabled efficient excitation of the mechanical mode, and hence of phonon lasing, when the spectral distance between the two supermodes was equal to the frequency of the mechanical mode supported in μR1. When this compound system was driven by an optical field with power above a certain threshold value, radiation-pressure-induced mechanical oscillations set in, leading to the modulation of the transmitted light at the frequency Ω_m of the mechanical motion (Fig. 1d). The radiofrequency (RF) spectrum of the modulated light provides information on the mechanical mode which is revealed by the peak located at Ω_m (Fig. 1e).

In the absence of the mechanical mode, the coupling between the optical modes a_1 of μR1 (the resonator supporting the mechanical motion) and a_2 of μR2 (the resonator without the mechanical motion) having the same frequency ω_0 creates two optical supermodes $a_\pm$ with complex eigenfrequencies $\omega_\pm = \omega_0 - i\chi \pm \beta$ where $\chi = (\gamma_1+\gamma_2)/2$ and $\beta = \sqrt{\kappa^2-\gamma^2}$ with $\gamma = (\gamma_2-\gamma_1)/2$. Here, κ is the coupling strength between the modes, $\gamma_1 = \gamma_{10}+\gamma_{c1}$ and $\gamma_2 = \gamma_{20}+\gamma_{tip}$ are the damping rates of the optical modes a_1 and a_2 with γ_{10} and γ_{20} representing their intrinsic damping rates, and γ_{c1}, γ_{tip} denote, respectively, the coupling loss of the taper–μR1 system and the additional loss introduced to μR2 by the nanotip. The point ($\kappa=\gamma$), where the eigenvalues of the system coalesce at $\omega_\pm = \omega_0 - i\chi$, corresponds to an EP at which the eigenvectors also coalesce. In the region before the EP ($\kappa>\gamma$), the supermodes have the same damping rate χ but different resonance frequencies $\omega_\pm = \omega_0 \pm \beta$ separated from each other by 2β. In the region after the EP ($\kappa<\gamma$), the supermodes have the same frequency ω_0 but different damping rates $\chi \mp i\beta$. In our experiments, where the coupling strength κ determined by the physical distance between the resonators was kept fixed, γ_{tip} was tuned to vary γ, which in turn allowed us to operate the system in three different regimes (before, after, and in the vicinity of the EP). From the experimentally obtained transmission spectra, we estimated the relevant parameters as $\kappa = 12.63$ MHz, $\gamma_{10} = 1.58$ MHz, $\gamma_{20} = 13.56$ MHz and $\gamma_{c1} = 1.58$ MHz.

Our experiments and the underlying physics of phonon lasing at an EP can be intuitively understood as follows (Fig. 2). Initially, the system is in the strong coupling regime (that is, before the EP) and the spectra exhibit two well-separated resonant modes (located at $\omega_\pm = \omega_0 \pm \beta$ with a spectral splitting of $2\beta \approx \Omega_m$), which are symmetrically distributed in the resonators (Fig. 2a). When the power of the pump laser with its frequency set around $\omega_+ = \omega_0 + \beta$ is above the threshold of mechanical oscillation, this mechanical oscillation in μR1 creates Stokes and anti-Stokes scattered photons with frequency $\omega_S = \omega_0 - \beta$ and $\omega_{aS} = \omega_0 + 3\beta$, respectively. Because ω_S lies within the frequency band of the resonance at $\omega_- = \omega_0 - \beta$, the amplitude of the Stokes sideband is resonantly enhanced. The amplitude of the anti-Stokes sideband, on the other hand, is suppressed because of the absence of a resonance at ω_{aS}. As a result, energy flows from photons to phonons in a highly efficient way due to resonantly enhanced

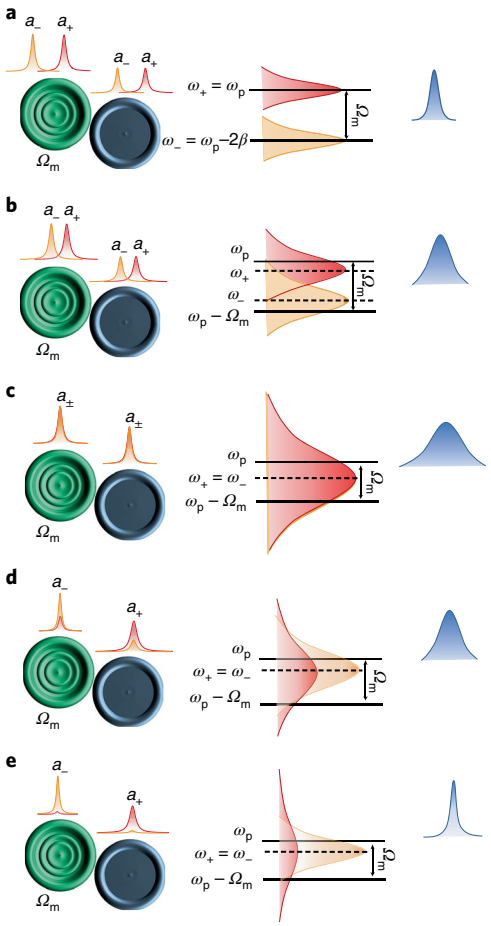

Fig. 2 | Tuning a phonon laser to an exceptional point. The first column shows a schematic of the distribution of the optical supermodes $a_\pm$ in the two resonators. The second column illustrates the frequency difference and linewidths of the two optical supermodes $a_\pm$. The last column represents the linewidth of the phonon laser. The damping rate γ_{tip} increases from **a** to **e**. **a**,**b**, The regime before the EP: the pump mode and the Stokes mode, which act as the analogue of a two-level atom, are within the frequency bands of the two optical supermodes respectively. The increasing γ_{tip} leads to the increase of the linewidths of the optical supermodes and to the decrease of the frequency difference between them. **c**, The EP at which the two optical supermodes are degenerate, and the pump mode and the Stokes mode are within the frequency bands of these two optical supermodes. The non-orthogonality of the optical modes introduces excess noise in the optical modes that reaches a maximum at the EP. Driven by the optical modes, the phonon laser inherits the increased optical noise, which is reflected by a broadened mechanical linewidth. **d**,**e**, The regime after the EP: the pump mode and the Stokes mode are within the frequency bands of the optical supermodes a_- and a_+ that are localized in the first and second resonators, respectively. The increasing γ_{tip} pushes the system away from the EP, leading to a linewidth narrowing of the phonon laser.

pumping of the system at ω_+ and resonantly enhanced collection of the Stokes photons at ω_-, resulting in coherent amplification of the mechanical oscillation. In this setting, the optical supermodes a_+ and a_- mimic a two-level system in which the transitions between the two levels are mediated by the mechanical mode, thereby creating a 'phonon laser'.

Introducing the nanotip, and hence inducing additional loss γ_{tip}, to μR2 moves the two supermodes spectrally closer to each other. Therefore, with increasing γ_{tip}, the system transits from well-separated and symmetrically distributed supermodes (Fig. 2a) to increasingly overlapping supermodes (Fig. 2b,c) with a complete overlap achieved at the EP (Fig. 2c). Further increase of γ_{tip} pushes the system beyond the EP, resulting in the strong localization of one of the supermodes in μR1 and the other in μR2 (Fig. 2d,e). Consequently, the mode in μR2 dissipates quickly owing to the presence of γ_{tip} while the mode in μR1 barely feels γ_{tip}. For the situation in which the supermodes overlap considerably (Fig. 2c–e), phonon lasing takes place because the resulting linewidth broadening of the overlapping modes is larger than the frequency of the mechanical mode. In the picture of a two-level system, this whole process corresponds to tuning the energy difference between the upper and lower energy levels such that with increasing γ_{tip} the upper and lower levels approach each other and become degenerate at an EP. As a result, during this process both the threshold and the linewidth of the phonon laser are affected (see our detailed discussion based on the experimental results below). First, increasing loss redistributes the supermodes between the resonators and alters the intracavity field intensity in μR1[13], which supports the mechanical mode, leading to a variation of the phonon lasing threshold such that the threshold first increases and then decreases as the system moves closer to the EP (Fig. 3). Second, the emitter (upper level) and collector (lower level) states are completely overlapping and non-orthogonal at the EP such that the enhancement of the noise in the optical modes becomes maximal. The noise inherent in these optical modes imprints on the phonon mode a linewidth that is maximally broadened at the EP (Fig. 4).

The behaviour of the phonon lasing threshold discussed above is seen in our experiments. Figure 3a depicts the RF signal power versus the optical pump power obtained at various values of γ_{tip}. In Fig. 3b, we present the threshold values as a function of the loss induced by the tip (that is, γ_{tip}). This shows that when γ_{tip} is increased, the threshold of the phonon laser first increases very slowly; after reaching a maximum value at a critical value of γ_{tip}, the threshold experiences a sudden drop. This behaviour is due to the loss-induced redistribution of the supermodes $a_\pm$ in the two resonators μR1 and μR2 when the system approaches the EP: in particular, when we increase the loss γ_{tip} such that the system approaches the EP, the intracavity field intensity in the high-Q resonator μR1 will first decrease to reach a minimum and then increase[13]. Because the phonon mode is located in the high-Q resonator μR1, this increase means that more energy can be transferred from the optical modes to the phonon mode for fixed input pump power such that the threshold of the phonon laser is decreased.

Next we focus on the central question: how is the linewidth of the phonon laser affected when it is operated near or at an EP? As shown in Fig. 4a, when the phonon laser was operated under different values of γ_{tip} while the pump power was tuned to keep the RF peak power of the phonon laser fixed, the linewidth of the phonon laser first increased in the regime before the EP but then decreased when the loss was further increased to move the system beyond the EP (into the regime after the EP). The phonon laser studied here is an analogue to a photon laser, but where, however, the lower and upper levels of a gain medium are replaced by two optical supermodes, and the photon-mediated transitions between the two levels are replaced by phonon-mediated transitions[38]. As discussed in detail in the Supplementary Information, the linewidth of the phonon laser can be calculated and represented in a similar way to a photon laser by taking into account the noise-induced phase diffusion process, resulting in the following approximate expression for the linewidth of the phonon laser

$$\Delta\nu \approx \Delta\nu_0 + \frac{\Gamma_m}{2n_{b,ss}}(2n_{spon} + 2n_{bT} + 1) \quad (1)$$

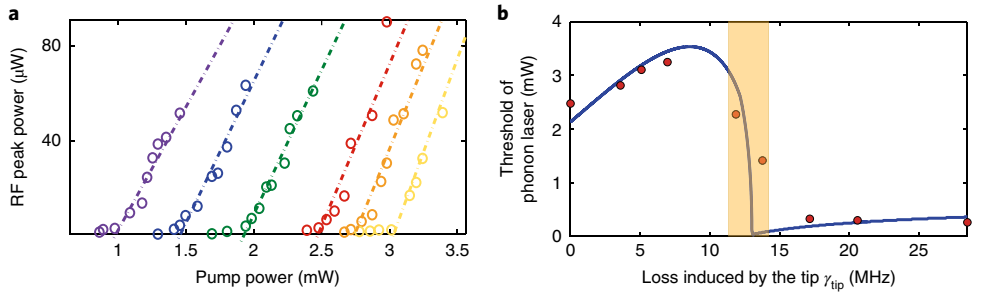

Fig. 3 | The threshold of the phonon laser before and after the exceptional point. a, Threshold curves of the phonon laser for different γ_{tip}. The damping rates for the threshold curves from left to right are γ_{tip} = 17.2 MHz, 13.8 MHz, 11.9 MHz, 0 MHz, 3.8 MHz and 6.9 MHz. **b**, The threshold of the phonon laser versus γ_{tip}. Before the EP, the threshold of the phonon laser increases with the increase of γ_{tip}, and then experiences a sudden drop in the vicinity of the EP. After the EP, the threshold of the phonon laser monotonously increases with the increase of γ_{tip}. The orange shaded area shows the region in the vicinity of the EP.

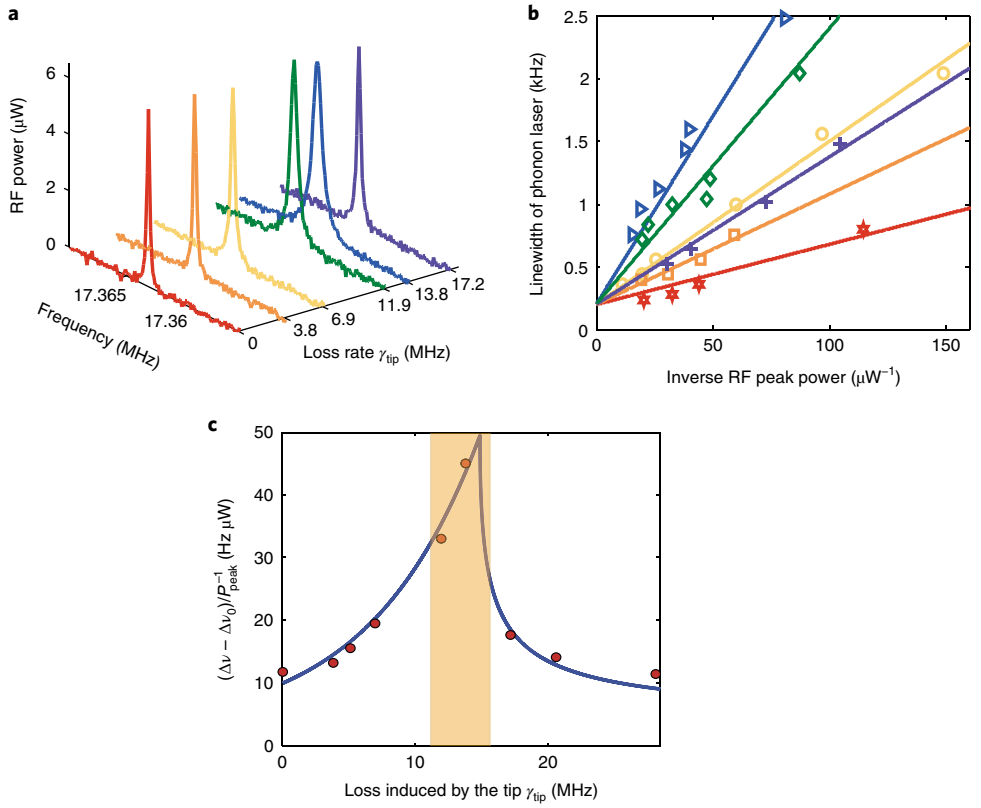

Fig. 4 | Linewidth enhancement of a phonon laser at an exceptional point. a, The power spectra of the phonon laser at different damping rates γ_{tip}. The linewidth of the phonon laser first increases and then decreases when we increase γ_{tip} from 0 MHz to 17.2 MHz. **b**, Linewidth versus inverse RF peak power of the phonon laser. Different curves correspond to different γ_{tip}. All the curves start from the same point with non-zero linewidth but feature different slopes. The damping rates for the curves from top to bottom are γ_{tip} = 13.8 MHz, 11.9 MHz, 6.9 MHz, 17.2 MHz, 3.8 MHz and 0 MHz. **c**, The red circles and the blue solid curve denote the experimental data points and a guide to the eye of the ratio between the normalized linewidth of the phonon laser and the inverse of the RF peak power $(\Delta\nu - \Delta\nu_0)/P_{peak}^{-1}$, which is enhanced in the vicinity of the EP (orange shaded area).

where $n_{b,ss}$ is the steady-state number of phonons, which is proportional to the RF peak power of the phonon laser P_{peak}, and $\Delta\nu_0$ is a phenomenological linewidth contribution taking into account all power-independent noise sources that are not included in our model. The factor n_{bT} represents the thermally excited phonons, and n_{spon} has been introduced in analogy to what is adopted in conventional laser theory, where it represents the number of spontaneously emitted photons into the cavity. In our phonon laser system, this factor n_{spon} is strongly enhanced when approaching the EP owing to the increasing noise in the optical supermodes, thereby creating a growing number of incoherent phonons in the mechanical resonator, which broaden the laser line (see the Supplementary Information for more details). We emphasize, however, that this increase of the linewidth in the vicinity of the EP has a different origin from that of a similar increase predicted for the photon laser. In the latter, the EP emerges because of overlapping modes of the optical resonator. In the phonon laser studied here, the EP emerges in the two-level system (that is, optical supermodes of the system)

where the transitions are mediated by phonons (that is, a mechanical mode). Quite remarkably, however, in both of these cases the EP leads to a considerable linewidth enhancement.

The linear dependence of the phonon laser linewidth $\Delta\nu$ on its inverse RF peak power (P_{peak}^{-1} proportional to $n_{\mathrm{b,ss}}^{-1}$) (see equation (1)) is clearly seen in our experimental results (Fig. 4b). In the limit of zero inverse output power $P_{\mathrm{peak}}^{-1} \to 0$ (that is, for strong output power), the linewidth $\Delta\nu$ approaches $\Delta\nu_0$, which is reflected in our experiments by the fact that for all different values of γ_{tip}, we found the same value of a power-independent linewidth $\Delta\nu_0 \approx 0.2\,\mathrm{kHz}$. As seen in Fig. 4c, the linewidth enhancement factor of the phonon laser given by $(\Delta\nu - \Delta\nu_0)/P_{\mathrm{peak}}^{-1}$ increases significantly as γ_{tip} is increased and the system moves closer to the EP. After passing the EP, the linewidth enhancement decreases again with further increase in γ_{tip}. For fixed RF peak power, we find that the linewidth of the phonon laser is enhanced at least five-fold at the EP. The underlying physics of this interesting behaviour can be understood as follows: when the system is steered towards the EP, the optical supermodes converge to each other, becoming more and more non-orthogonal until they are fully parallel at the EP. As can be shown in a simple scattering matrix model[26], the non-orthogonality of the optical modes leads to a marked increase of the effective optical noise and with it to a broadening of the optical linewidth (as inherent in the Petermann factor) that reaches a maximum directly at the EP (see the Supplementary Information for details). As, in our system, the phonon mode is driven by these noisy optical modes, the increased optical noise transfers directly to a mechanical excess noise and consequently leads to a broadening of the mechanical linewidth. In this sense, the phononic mode in our set-up may be interpreted as a probe of the optical noise in the optical supermodes. While these results imply that the coherence of the phonon laser is decreased in the vicinity of an EP, they also show that one can tune the linewidth of the phonon laser by moving it closer to or away from an EP. This may be useful for applications in which the linewidth or coherence of the phonon laser are of importance.

This work differs from ref.[13] in many ways, in particular in the physical mechanism behind the observations, although in both cases the system is brought to the vicinity of an EP by additionally introduced losses. The most relevant differences are the following. First, ref.[13] considers a Raman laser (optical photons with a frequency in the terahertz regime) whereas the current work considers a phonon laser (amplification of mechanical mode, and phonons in the megahertz frequency regime). Second, in ref.[13] the gain for the laser is provided by the Raman process in silica, and the additionally induced loss does not affect the gain mechanism; it just redistributes the energy between supermodes by bringing the coupled resonator system to and away from an EP. In this work, the additional loss does affect the gain medium, by bringing the two-level system (the gain system) to and away from an EP where the energy levels of the two-level system coalesce. Thus, whereas in ref.[13] the EP emerges in the optical modes driving the gain mechanism, in this work the EP emerges in the spectra of the gain medium. Third, ref.[13] reports loss-induced suppression and revival of a Raman laser before and after an EP without any reference to the effect of the EP on the linewidth of the Raman laser. The current work, on the other hand, focuses on the effect of an EP on the linewidth of a phonon laser and reports the observation of linewidth broadening in this new context.

In summary, we have experimentally investigated a phonon laser to provide insights into the long-debated issue of how a laser—in particular its linewidth—is affected when being operated at an EP. By steering the phonon laser close to the EP, we have shown that its linewidth is greatly enhanced. This broadening is attributed to the increased noise in the two optical supermodes that provide the gain for the phonon laser and that increasingly overlap when approaching the EP. Our study provides direct experimental evidence showing that EP-enhanced optical noise can be transferred directly to mechanical noise, leading to a linewidth broadening in phonon lasers. It opens up new perspectives for the relation between noise and non-Hermitian physics and may find applications in various related fields such as signal processing technologies. For example, our system could be used as an on-chip phononic device, similar to fully integrated photonic devices, which are widely used for information processing. Even more interestingly, the studied platform can provide insight into EPs in two-level or multi-level systems and into their detection and control.

Data availability. The data that support the plots within this paper and other findings of this study are available from the corresponding author upon reasonable request.

Received: 14 August 2017; Accepted: 7 June 2018;
Published online: 09 July 2018

References

1. Bender, C. M. Making sense of non-Hermitian Hamiltonians. *Rep. Prog. Phys.* **70**, 947–1018 (2007).
2. Moiseyev, N. *Non-Hermitian Quantum Mechanics* (Cambridge Univ. Press, Cambridge, 2011).
3. Doppler, J. et al. Dynamically encircling an exceptional point for asymmetric mode switching. *Nature* **537**, 76–79 (2016).
4. Dembowski, C. et al. Experimental observation of the topological structure of exceptional points. *Phys. Rev. Lett.* **86**, 787–790 (2001).
5. Guo, A. et al. Observation of PT-symmetry breaking in complex optical potentials. *Phys. Rev. Lett.* **103**, 093902 (2009).
6. Rüter, C. E. et al. Observation of parity–time symmetry in optics. *Nat. Phys.* **6**, 192–195 (2010).
7. Klaiman, S., Günther, U. & Moiseyev, N. Visualization of branch points in PT-symmetric waveguides. *Phys. Rev. Lett.* **101**, 080402 (2008).
8. Lin, Z. et al. Unidirectional invisibility induced by PT-symmetric periodic structures. *Phys. Rev. Lett.* **106**, 213901 (2011).
9. Regensburger, A. et al. Parity–time synthetic photonic lattices. *Nature* **488**, 167–171 (2012).
10. Peng, B. et al. Parity–time-symmetric whispering-gallery microcavities. *Nat. Phys.* **10**, 394–398 (2014).
11. Chang, L. et al. Parity–time symmetry and variable optical isolation in active–passive-coupled microresonators. *Nat. Photon.* **8**, 524–529 (2014).
12. Peng, B. et al. Chiral modes and directional lasing at exceptional points. *Proc. Natl Acad. Sci. USA* **113**, 6845–6850 (2016).
13. Peng, B. et al. Loss-induced suppression and revival of lasing. *Science* **346**, 328–332 (2014).
14. Feng, L., Wong, Z. J., Ma, R.-M., Wang, Y. & Zhang, X. Single-mode laser by parity–time symmetry breaking. *Science* **346**, 972–975 (2014).
15. Hodaei, H., Miri, M.-A., Heinrich, M., Christodoulides, D. N. & Khajavikhan, M. Parity–time-symmetric microring lasers. *Science* **346**, 975–978 (2014).
16. Wiersig, J. Enhancing the sensitivity of frequency and energy splitting detection by using exceptional points: application to microcavity sensors for single-particle detection. *Phys. Rev. Lett.* **112**, 203901 (2014).
17. Liu, Z.-P. et al. Metrology with PT-symmetric cavities: enhanced sensitivity near the PT-phase transition. *Phys. Rev. Lett.* **117**, 110802 (2016).
18. Chen, W., Özdemir, S. K., Zhao, G., Wiersig, J. & Yang, L. Exceptional points enhance sensing in an optical microcavity. *Nature* **548**, 192–196 (2017).
19. Hodaei, H. et al. Enhanced sensitivity at higher-order exceptional points. *Nature* **548**, 187–191 (2017).
20. Xu, H., Mason, D., Jiang, L. & Harris, G. E. Topological energy transfer in an optomechanical system with exceptional points. *Nature* **537**, 80–83 (2016).
21. Wenzel, H., Bandelow, U., Wunsche, H. J. & Rehberg, J. Mechanisms of fast self pulsations in two-section DFB lasers. *IEEE J. Quantum Electron.* **32**, 69–78 (1996).
22. Berry, M. Mode degeneracies and the Petermann excess-noise factor for unstable lasers. *J. Mod. Opt.* **50**, 63–81 (2003).
23. Schawlow, A. L. & Townes, C. H. Infrared and optical masers. *Phys. Rev.* **112**, 1940–1948 (1958).
24. Peterman, K. Calculated spontaneous emission factor for double-heterostructure injection lasers with gain-induced waveguiding. *IEEE J. Quantum Electron.* **QE-15**, 566–570 (1979).
25. Siegman, A. E. Excess spontaneous emission in non-Hermitian optical systems. I. Laser amplifiers. *Phys. Rev. A* **39**, 1253–1263 (1989).
26. Grangier, P. & Poizat, J. P. A simple quantum picture for the Petermann excess noise factor. *Eur. Phys. J. D* **1**, 97–104 (1998).
27. Hamel, W. A. & Woerdman, J. P. Observation of enhanced fundamental linewidth of a laser due to nonorthogonality of its longitudinal eigenmodes. *Phys. Rev. Lett.* **64**, 1506 (1990).

28. Cheng, Y.-J., Fanning, C. G. & Siegman, A. E. Experimental observation of a large excess quantum noise factor in the linewidth of a laser oscillator having nonorthogonal modes. *Phys. Rev. Lett.* **77**, 627–630 (1996).
29. van Eijkelenborg, M. A., Lindberg, Å. M., Thijssen, M. S. & Woerdman, J. P. Resonance of quantum noise in an unstable cavity laser. *Phys. Rev. Lett.* **77**, 4314–4317 (1996).
30. Schomerus, H., Frahm, K. M., Patra, M. & Beenakker, C. W. J. Quantum limit of the laser line width in chaotic cavities and statistics of residues of scattering matrix poles. *Phys. A* **278**, 469–496 (2000).
31. Lee, S.-Y. et al. Divergent Petermann factor of interacting resonances in a stadium-shaped microcavity. *Phys. Rev. A* **78**, 015805 (2008).
32. Yoo, G., Sim, H.-S. & Schomerus, H. Quantum noise and mode nonorthogonality in non-Hermitian PT-symmetric optical resonators. *Phys. Rev. A* **84**, 063833 (2011).
33. Schomerus, H. Excess quantum noise due to mode nonorthogonality in dielectric microresonators. *Phys. Rev. A* **79**, 061801(R) (2009).
34. Chong, Y. D. & Douglas Stone, A. General linewidth formula for steady-state multimode lasing in arbitrary cavities. *Phys. Rev. Lett.* **109**, 063902 (2012).
35. Pick, A. et al. Ab initio multimode linewidth theory for arbitrary inhomogeneous laser cavities. *Phys. Rev. A* **91**, 063806 (2015).
36. Liertzer, M. et al. Pump-induced exceptional points in lasers. *Phys. Rev. Lett.* **108**, 173901 (2012).
37. Brandstetter, M. et al. Reversing the pump dependence of a laser at an exceptional point. *Nat. Commun.* **5**, 4034 (2014).
38. Grudinin, I. S., Lee, H., Painter, O. & Vahala, K. J. Phonon laser action in a tunable two-level system. *Phys. Rev. Lett.* **104**, 083901 (2010).
39. Jing, H. et al. PT-symmetric phonon laser. *Phys. Rev. Lett.* **113**, 053604 (2014).
40. Cartarius, H., Main, J. & Wunner, G. Exceptional points in atomic spectra. *Phys. Rev. Lett.* **99**, 173003 (2007).

Acknowledgements

This work was supported by NSF grant no. EFMA1641109, ARO grant no. W911NF1210026, ARO grant no. W911NF1710189 and the European Commission under project NHQWAVE (MSCA-RISE 691209). S.K.O. was supported by ARO grant no. W911NF-16-1-0339. S.K.O thanks J. Mateo for his continuous support. J.Z. is supported by the NSFC under grant nos. 61622306, 11674194. Y.-X.L. is supported by the NSFC under grant no. 61025022. Y.-X.L. and J.Z. are supported by the National Basic Research Program of China (973 Program) under grant no. 2014CB921401, the Tsinghua University Initiative Scientific Research Program and the Tsinghua National Laboratory for Information Science and Technology (TNList) Cross-discipline Foundation. F.N. is partially supported by the MURI Center for Dynamic Magneto-Optics via AFOSR Award no. FA9550-14-1-0040, Asian Office of Aerospace Research and Development (AOARD) (grant no. FA2386-18-1-4045), the IMPACT program of JST, JSPS-RFBR grant no. 17-52-50023, CREST grant no. JPMJCR1676, RIKEN-AIST Joint Research Fund and the Sir John Templeton Foundation. K.P., D.O.K. and S.R. are supported by the Austrian Science Fund (FWF) through project no. SFB NextLite F49-P10. H. Yilmaz prepared the chromium-coated silica nanofibre tip for the experiments.

Author contributions

S.R., S.K.O, B.P. and L.Y. conceived the idea. B.P., J.Z., S.K.O., S.R. and L.Y. designed the experiments. J.Z and B.P. performed the experiments with help from G.Z. J.Z. analysed the experimental data, J.Z., K.P. and D.O.K. performed the theoretical analysis and numerical simulations, guided by S.K.O, Y.-X.L. and S.R. J.Z., S.K.O., S.R., Y.-X.L. and L.Y. wrote the manuscript with contributions from all authors. L.Y. supervised the research.

Competing interests

The authors declare no competing interests.

Additional information

Supplementary information is available for this paper at https://doi.org/10.1038/s41566-018-0213-5.

Reprints and permissions information is available at www.nature.com/reprints.

Correspondence and requests for materials should be addressed to L.Y.

Publisher's note: Springer Nature remains neutral with regard to jurisdictional claims in published maps and institutional affiliations.

nature photonics

SUPPLEMENTARY INFORMATION

https://doi.org/10.1038/s41566-018-0213-5

In the format provided by the authors and unedited.

A phonon laser operating at an exceptional point

Jing Zhang[1,2,3,10], Bo Peng[1,8,10], Şahin Kaya Özdemir[1,9], Kevin Pichler[4], Dmitry O. Krimer[4], Guangming Zhao[1], Franco Nori[5,6], Yu-xi Liu[3,7], Stefan Rotter[4] and Lan Yang[1*]

[1]Department of Electrical and Systems Engineering, Washington University, St Louis, MO, USA. [2]Department of Automation, Tsinghua University, Beijing, China. [3]Center for Quantum Information Science and Technology, BNRist, Beijing, China. [4]Institute for Theoretical Physics, Vienna University of Technology (TU Wien), Vienna, Austria. [5]Theoretical Quantum Physics Laboratory, RIKEN, Saitama, Japan. [6]Physics Department, The University of Michigan, Ann Arbor, MI, USA. [7]Institute of Microelectronics, Tsinghua University, Beijing, China. [8]Present address: IBM Thomas J. Watson Research Center, Yorktown Heights, NY, USA. [9]Present address: Department of Engineering Science and Mechanics, The Pennsylvania State University, University Park, PA, USA. [10]These authors contributed equally: Jing Zhang, Bo Peng. *e-mail: yang@seas.wustl.edu

Supplementary Information – A phonon laser operating at an exceptional point

Jing Zhang[1,2,3], Bo Peng[1†], Şahin Kaya Özdemir[1†], Kevin Pichler[4], Dmitry O. Krimer[4], Guangming Zhao[1], Franco Nori[5,6], Yu-xi Liu[3,7], Stefan Rotter[4], & Lan Yang[1*]

Affiliations:

[1]Department of Electrical and Systems Engineering, Washington University, St. Louis, Missouri 63130, USA

[2]Department of Automation, Tsinghua University, Beijing 100084, P. R. China

[3]Center for Quantum Information Science and Technology, BNRist, Beijing 100084, P. R. China

[4]Institute for Theoretical Physics, Vienna University of Technology (TU Wien), Vienna, Austria, EU

[5]Theoretical Quantum Physics Laboratory, RIKEN, Saitama 351-0198, Japan

[6]Physics Department, The University of Michigan, Ann Arbor, MI 48109-1040, USA

[7]Institute of Microelectronics, Tsinghua University, Beijing 100084, P. R. China

[†]Present address: IBM Thomas J. Watson Research Center, Yorktown Heights, New York 10598, USA (B.P.); Department of Engineering Science and Mechanics, The Pennsylvania State University, University Park, Pennsylvania 16802 USA (S.K.O.).

*email: yang@seas.wustl.edu

I. EXPERIMENTAL SETUP

Our experiment was performed using the setup illustrated in Fig. S1. An optical probe field provided by a tunable External Cavity Laser Diode (ECLD) in the 1550 nm band was fed into the fiber. A section of the fiber was tapered to enable efficient coupling of the probe field into and out of a microtoroid resonator, which is coupled to another microtoroid resonator with tunable damping rate induced by a chromium (Cr)-coated silica-nanofiber tip with strong absorption rate of light in the 1550-nm band, and the output field was sent to a Photo-Detector (PD). The electrical signal from the PD was then analyzed

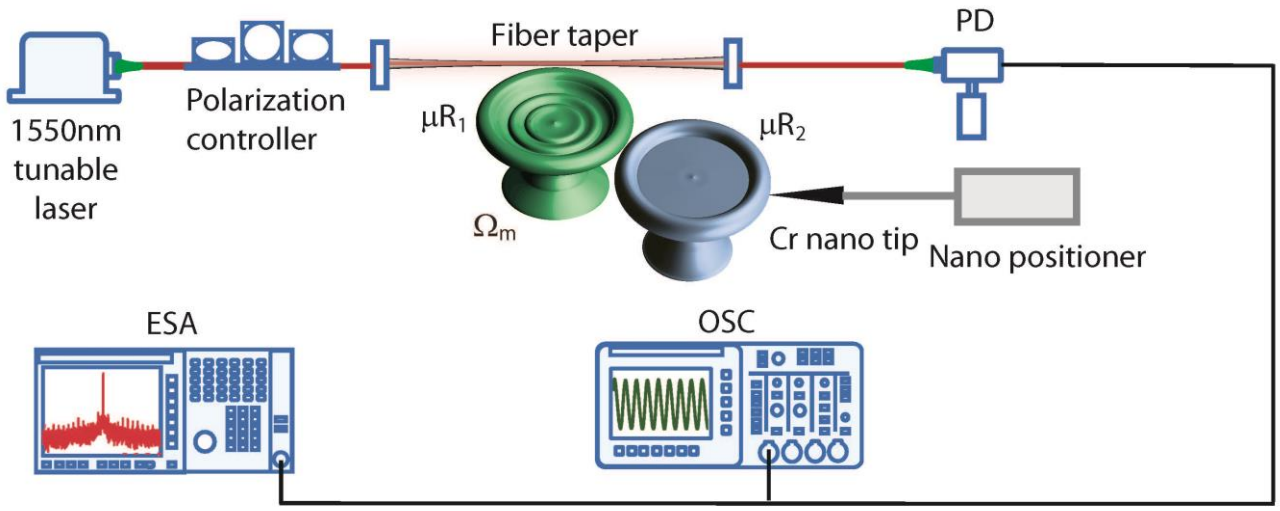

Figure S1. Schematic diagram of the experimental setup. The 1550 nm laser is fed into two coupled microtoroid resonators μR1 and μR2. The first resonator μR1 supports a high-Q optical mode a_1 and a mechanical mode with frequency Ω_m, while the second resonator μR2 supports a low-Q mode a_2. The damping rate of the low-Q mode a_2 is tuned by a Cr-coated silica nanotip touching the resonator μR2. The output signal is detected by a photodetector and then fed into the oscilloscope and the electrical spectrum analyzer to obtain the time and frequency domain signals for the mechanical mode. PD: photodetector; OSC: oscilloscope; ESA: Electrical spectrum analyzer.

with an oscilloscope in order to monitor the time-domain behavior, and also with an Electrical Spectrum Analyzer (ESA) to obtain the power spectra.

II. BIFURCATION IN THE VICINITY OF THE EXCEPTIONAL POINT

For the compound phonon laser system considered in this work, there exists an exceptional point for the optical modes in the coupled resonators and a bifurcation occurs in the vicinity of this exceptional point. In fact, the coupling between the two optical modes a_1 and a_2 in the two resonators with strength κ gives rise to two optical supermodes $a_\pm$ with complex eigenfrequencies $\omega_\pm = \Delta\omega - i\chi \pm \beta$ (in a frame rotating with ω_p) where $\Delta\omega=\omega_0-\omega_p$ is the detuning between the optical pump frequency ω_p and the cavity resonance frequency ω_0, $\chi=(\gamma_1+\gamma_2)/2$, $\beta=\sqrt{\kappa^2-\gamma^2}$, and $\gamma=(\gamma_2-\gamma_1)/2$. $\gamma_1=\gamma_{10}+\gamma_{c1}$ and $\gamma_2=\gamma_{20}+\gamma_{\text{tip}}$ represent the damping rates of a_1 and a_2. γ_{10} and γ_{20} are the intrinsic damping rates of a_1 and a_2 induced e.g. by the material absorption, scattering, and radiation losses. γ_{c1} is the damping rate of a_1 induced by the coupling between the resonator and the fiber-taper and γ_{tip} is the additional loss induced by the nanotip. When $\gamma<\kappa$, the two supermodes are non-degenerate with frequencies $\Delta\omega\pm\beta$ and the same damping rate χ (see Fig. S2a and Fig. S2b). This case is referred to as the regime before the exceptional point. On the other hand, when $\gamma>\kappa$, the two supermodes are degenerate with frequency $\Delta\omega$ but different damping rates $\chi\pm i\beta$ (see Fig. S2a and Fig. S2b), which is referred to as the regime after the exceptional point. At $\kappa=\gamma$, i.e., at the exceptional point, the two supermodes are degenerate with equal damping rate, indicating a transition between the regime before the exceptional point and the regime after the exceptional point. In Fig. S2c-S2e we show the output spectra of the optical supermodes which exhibit the degeneracy of the optical modes at the exceptional point.

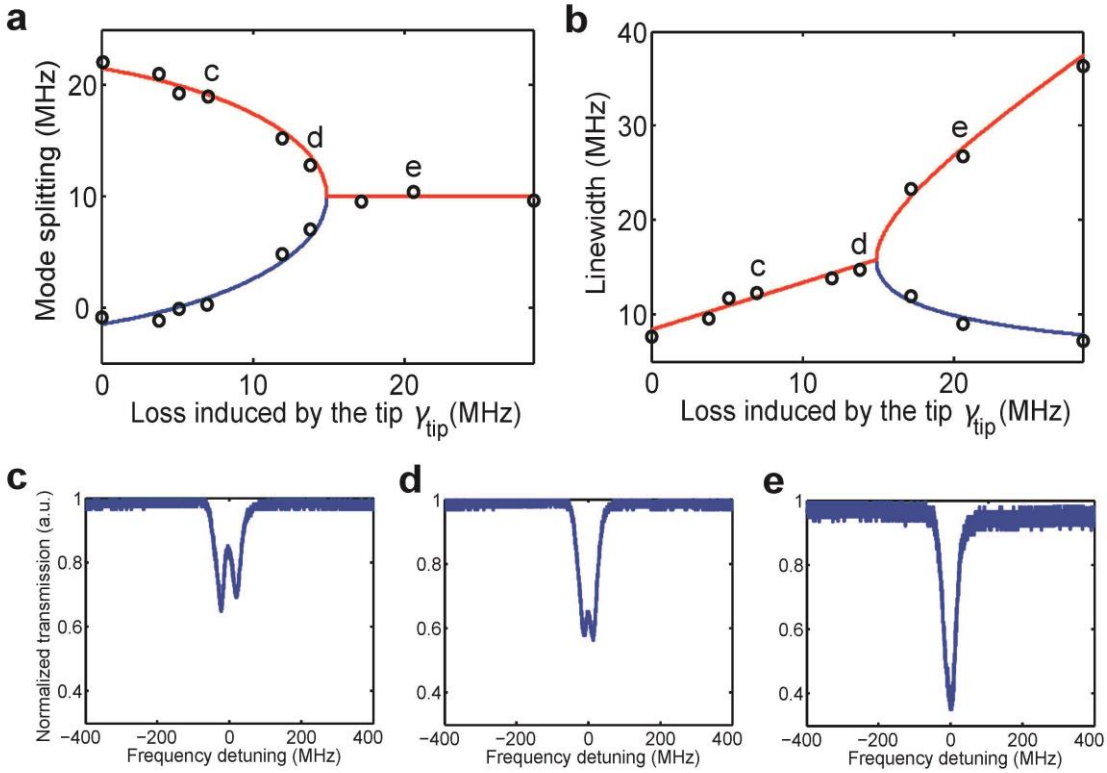

Figure S2. Bifurcation in the vicinity of the exceptional point in the compound phonon laser system. a, Real part of the eigenfrequencies of the optical supermodes as a function of the loss induced by the nanotip γ_{tip}, which shows the mode splitting and coalescence in the vicinity of the exceptional point. **b**, Imaginary part of the eigenfrequencies of the optical supermodes as a function of the loss induced by the nanotip γ_{tip}, which illustrates the linewidth bifurcation of the optical supermodes. **c-e**, Output spectra of the optical supermodes (c) before the exceptional point, which features mode splitting, (d) in the vicinity of the exceptional point, which shows overlapping optical supermodes with equal linewidths, and (e) after the exceptional point, where the optical supermodes are overlapping with different linewidths. Note that only the high-Q supermode, which is localized in the high-Q resonator in the regime after the exceptional point, can be seen in the output spectrum, the parameters for the low-Q supermode can be estimated indirectly from the theoretical model and those of the high-Q mode.

III. THRESHOLD OF THE PHONON LASER

To understand the physical mechanism behind the phonon laser, let us compare it with the one-dimesional cavity-mediated optical laser system shown in Fig. S3a, which is composed of an optical cavity with one fully-reflecting mirror at one end and a partially-reflecting mirror at the other end. The input pump field leads to the population inversion of the gain medium uniformally distributed in the cavity, and coherent photons are generated by the stimulated emission process which leads to the laser output. Figure S3b shows a picture of the lasing process in which coherent photons are generated by the interaction between the optical mode and the effective two-level atoms in the gain medium. The phonon laser in our system is somewhat similar to this picture of an optical laser to the extent that two optical supermodes act as a two-level system interacting with the phonon field. The mechanical mode supported by the microtoroid resonator interacts with the analog "two-level system" generated by the optical supermodes to receive phonon gain, and then suffers loss during transmission (see Fig. S3c and Fig. S3d). The balance between mechanical gain and mechanical loss leads to the phonon laser demonstrated in the experiments. Due to the similarity between the working principle of a phonon laser and that of an optical laser, one can derive the expressions for the threshold and the linewidth of the phonon laser following the approach carried out for an optical laser.

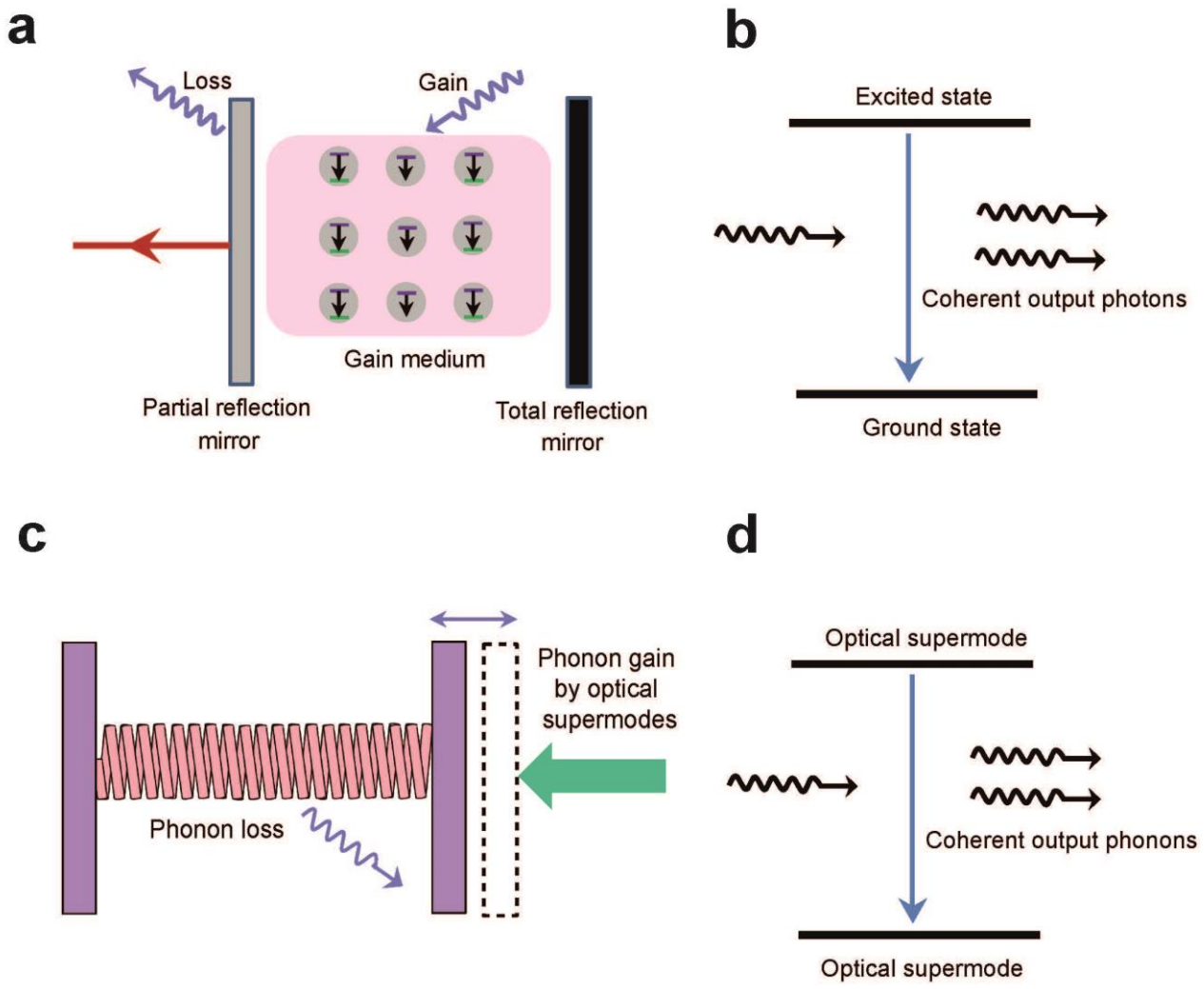

Figure S3. Comparison of an optical laser and a phonon laser. a, Diagram of a one-dimensional optical laser with a gain medium distributed in an optical cavity with one fully-reflecting mirror at one end and a patially-reflecting mirror at the other end. **b**, Mechanism of an optical laser, in which an optical mode interacts with a gain medium and coherent output photons are generated. **c**, Equivalent one-dimensional phonon laser with gain provided by the optical supermodes acting as a "two-level system". **d**, Equivalent mechanism of the phonon laser in which the mechanical mode interacts with the analog two-level system represented by the optical supermodes such that coherent output phonons are generated.

In the following, we perform the derivation of the threshold of the phonon laser. Denoting the intracavity fields of the two resonators as a_1 and a_2 in a frame rotating with the frequency of the driving field, and the phonon mode as b, the dynamical equations for our system can be written as

$$\frac{d}{dt}a_1 = \left[-\gamma_1 + i\left(\omega_p - \omega_1\right)\right]a_1 - i\kappa a_2 - ig_{om}a_1\left(b + b^*\right) + \sqrt{2\gamma_{c1}}\varepsilon, \tag{S.1}$$

$$\frac{d}{dt}a_2 = -i\kappa a_1 + \left[-\gamma_2 + i\left(\omega_p - \omega_2\right)\right]a_2, \tag{S.2}$$

$$\frac{d}{dt}b = -\left(\Gamma_m + i\Omega_m\right)b - ig_{\mathrm{om}}a_1^* a_1, \tag{S.3}$$

where ω_1 and ω_2 are the cavity-mode line center frequencies of a_1 and a_2, ω_p is the frequency of the driving field, g_{om} is the optomechanical coupling strength, and ε is the amplitude of the input field fed into the first resonator. $\gamma_1 = \gamma_{10} + \gamma_{c1}$ and $\gamma_2 = \gamma_{20} + \gamma_{\mathrm{tip}}$ represent the damping rates of a_1 and a_2, in which γ_{10} and γ_{20} are the intrinsic damping rates of a_1 and a_2, γ_{c1} is the damping rate of a_1 induced by the coupling between the resonator and the fiber-taper, and γ_{tip} is the additional loss induced by the nanotip. Ω_m and Γ_m are the frequency and damping rate of the mechanical mode. The two optical fields a_1 and a_2 couple to each other via the evanescent field with coupling strength κ, which gives rise to two optical supermodes

$$\begin{pmatrix} a_+ \\ a_- \end{pmatrix} = \begin{pmatrix} \mathcal{N}_-^{-1} & \\ & \mathcal{N}_+^{-1} \end{pmatrix} \begin{pmatrix} \tau_+ & \tau_- \\ 1 & 1 \end{pmatrix}^{-1} \begin{pmatrix} a_1 \\ a_2 \end{pmatrix} = \begin{pmatrix} \mathcal{N}_-^{-1} & \\ & \mathcal{N}_+^{-1} \end{pmatrix} \begin{pmatrix} \mu & -\lambda_- \\ -\mu & \lambda_+ \end{pmatrix} \begin{pmatrix} a_1 \\ a_2 \end{pmatrix} \tag{S.4}$$

with complex eigenfrequencies

$$\omega_\pm = -\Delta_+ - i\chi \pm \sqrt{\kappa^2 + \left(\Delta_- + i\gamma\right)^2}, \tag{S.5}$$

where $\chi=(\gamma_1+\gamma_2)/2$, $\beta+i\tilde{\beta}=\sqrt{\kappa^2-\gamma^2}$, $\gamma=(\gamma_2-\gamma_1)/2$, $\Delta_\pm=\left[(\omega_p-\omega_1)\pm(\omega_p-\omega_2)\right]/2$, and

$$\tau_\pm=\frac{\Delta_-+i\gamma}{\kappa}\pm\sqrt{1+\left(\frac{\Delta_-+i\gamma}{\kappa}\right)^2},$$

$$\mu=\frac{1}{\tau_+-\tau_-}=\frac{\kappa}{2\left[\kappa^2+(\Delta_-+i\gamma)^2\right]^{1/2}},$$

$$\lambda_\pm=\frac{\tau_\pm}{\tau_+-\tau_-}=\frac{\Delta_-+i\gamma\pm\left[\kappa^2+(\Delta_-+i\gamma)^2\right]^{1/2}}{2\left[\kappa^2+(\Delta_-+i\gamma)^2\right]^{1/2}}. \tag{S.6}$$

$\mathcal{N}_\pm$ are normalization constants which are given by

$$\mathcal{N}_\pm=\sqrt{|\mu|^2+|\lambda_\pm|^2}.$$

Note that we have omitted the influence of the nonlinear optomechanical coupling for writing down the expressions for the optical supermodes under the assumption that the optomechanical coupling strength is weak, which has been widely used in the existing phonon laser literature [S1]-[S5]. For the case with strong optomechanical coupling, the mechanical mode would induce additional detuning and thus shift the optical supermodes [S6] which is not considered in our discussions. Since the physical phenomena that we are interested in appear in the regime where the system is in the vicinity of the exceptional point, we will mainly focus on this regime in the following discussions.

a. The regime before the exceptional point $\gamma\leq\kappa$

Let us first consider the regime before the exceptional point in which $\beta\neq 0$, $\tilde{\beta}=0$ and assume that the intracavity resonance frequencies of the two resonators are degenerate, i.e. $\omega_1=\omega_2\triangleq\omega_0$. In this case, the two optical supermodes can be simplified according to

$$\begin{aligned}\begin{pmatrix} a_+ \\ a_- \end{pmatrix} &= \frac{\sqrt{2}\beta}{\kappa}\begin{pmatrix} (\beta+i\gamma)/\kappa & (-\beta+i\gamma)/\kappa \\ 1 & 1 \end{pmatrix}^{-1}\begin{pmatrix} a_1 \\ a_2 \end{pmatrix} \\ &= \frac{\sqrt{2}\beta}{\kappa}\begin{pmatrix} \mu & -\lambda_- \\ -\mu & \lambda_+ \end{pmatrix}\begin{pmatrix} a_1 \\ a_2 \end{pmatrix}\end{aligned} \tag{S.7}$$

with complex eigenfrequencies

$$\omega_\pm = \omega_0 - \omega_p \pm \beta - i\chi, \tag{S.8}$$

where

$$\mu = \frac{\kappa}{2\beta}, \quad \lambda_\pm = \frac{i\gamma \pm \beta}{2\beta}. \tag{S.9}$$

If we omit the self-frequency-shift terms $a_+^* a_+ \left(b + b^*\right)$ and $a_-^* a_- \left(b + b^*\right)$ and non-resonant terms like $a_-^* a_+ b$ and $a_+^* a_- b^*$ in the Hamiltonian of the optomechanical coupling, the dynamical equations for the optical supermodes $a_\pm$ can be expressed as [S1], [S2]

$$\frac{d}{dt}a_- = -\left[\chi + i\left(\omega_0 - \omega_p - \beta\right)\right]a_- + ig_{\mathrm{om}}\frac{i\gamma - \beta}{2\beta}a_+ b^* + \sqrt{2\gamma_{c1}}\tilde{\varepsilon}, \tag{S.10}$$

$$\frac{d}{dt}a_+ = -\left[\chi + i\left(\omega_0 - \omega_p + \beta\right)\right]a_+ - ig_{\mathrm{om}}\frac{i\gamma + \beta}{2\beta}a_- b - \sqrt{2\gamma_{c1}}\tilde{\varepsilon}, \tag{S.11}$$

$$\frac{d}{dt}b = -\left(\Gamma_m + i\Omega_m\right)b - ig_{\mathrm{om}}\frac{\left(\gamma + i\beta\right)^2}{2\beta^2}a_-^* a_+, \tag{S.12}$$

where $\tilde{\varepsilon} = \left(\sqrt{2}\beta\mu\varepsilon\right)\Big/\kappa = \varepsilon/\sqrt{2}$. Note that here we have omitted the anti-Stokes mode which is out of the frequency bands of the two optical supermodes $a_\pm$.

The optical supermodes a_+ and a_- mimic a two-level system where the transitions between the energy levels are mediated by the mechanical mode, which gives rise to the phonon laser. To illustrate this, we define the ladder operators and population inversion quantities by the optical modes a_+ and a_- as

$$J_+ = a_+^* a_-, \qquad J_- = a_-^* a_+, \qquad J_z = a_+^* a_+ - a_-^* a_-, \tag{S.13}$$

From Eqs. (S.10)-(S.12) and taking the stationary states of the supermodes in the driving terms acting on the "two-level system", we have [S1], [S2]

$$\dot{J}_- = -2(\chi + i\beta)J_- + i\tilde{g}_{om} b J_z, \tag{S.14}$$

$$\dot{J}_+ = -2(\chi - i\beta)J_+ - i\tilde{g}^*_{om} b^* J_z, \tag{S.15}$$

$$\dot{J}_z = -2\chi J_z + 2i\tilde{g}^*_{om} b^* J_- - 2i\tilde{g}_{om} b J_+ + \Lambda, \tag{S.16}$$

$$\dot{b} = -(\Gamma_m + i\Omega_m)b - ig_{om}\frac{(\gamma + i\beta)^2}{2\beta^2} J_-. \tag{S.17}$$

$\tilde{g}_{om}$ denotes the effective optomechanical coupling strength in the supermode picture given by

$$\tilde{g}_{om} = g_{om}\frac{i\gamma + \beta}{2\beta}, \tag{S.18}$$

which already takes very large values in the vicinity of an exceptional point (i.e., very small non-zero values of β). While this observation implies EP-enhanced optomechanical interaction, the divergence of (S.18) directly at the EP ($\beta = 0$) also indicates that more terms are required to describe this parameter regime correctly. Λ is the effective pumping acting on the two-level system which can be expressed as

$$\Lambda = \sqrt{2\gamma_{c1}}\left(\tilde{\varepsilon}^* a_{ss,+} + a^*_{ss,+}\tilde{\varepsilon} + \tilde{\varepsilon}^* a_{ss,-} + a^*_{ss,-}\tilde{\varepsilon}\right), \tag{S.19}$$

where $a_{ss,+}$ and $a_{ss,-}$ are the stationary values of the supermodes $a_\pm$ from Eqs. (S.10) and (S.11). The factor 2 in the denominator of Eq. (S.18) comes from the fact that g_{om} is defined as the optomechanical coupling strength in the solitary resonator (i.e., single travelling mode in the resonator with mechanical mode) while $\tilde{g}_{om}$ in Eq. (S.18) is defined for the supermodes formed in the coupled resonators system.

Note that here we have omitted the driving terms acting on the dynamics of J_- and J_+ since we assume that the total population distribution of the two energy levels $n_+ + n_- = a^*_+ a_+ + a^*_- a_-$ is conserved, an

approximation which has already been introduced in previous phonon laser papers [S1]-[S5]. Transferring the variables to the rotating frame by setting $\tilde{b}=\exp\left(i\Omega_m t\right)b$, $\tilde{J}_-=\exp\left(i\Omega_m t\right)J_-$, and $\tilde{J}_+=\exp\left(-i\Omega_m t\right)J_+$, Eqs. (S.14)-(S.17) can be rewritten as

$$\dot{\tilde{J}}_-=-2\left[\chi-i\left(\Omega_m/2-\beta\right)\right]\tilde{J}_-+i\tilde{g}_{om}J_z\tilde{b}, \tag{S.20}$$

$$\dot{\tilde{J}}_+=-2\left[\chi+i\left(\Omega_m/2-\beta\right)\right]\tilde{J}_+-i\tilde{g}_{om}^*\tilde{b}^*J_z, \tag{S.21}$$

$$\dot{J}_z=-2\chi J_z+2i\tilde{g}_{om}^*\tilde{b}^*\tilde{J}_--2i\tilde{g}_{om}\tilde{b}\tilde{J}_++\Lambda, \tag{S.22}$$

$$\dot{\tilde{b}}=-\Gamma_m\tilde{b}-ig_{om}\frac{\left(\gamma+i\beta\right)^2}{2\beta^2}\tilde{J}_-. \tag{S.23}$$

We can adiabatically eliminate the degrees of freedom of the optical modes by setting $\dot{\tilde{J}}_-=0$ due to the reason that $\Gamma_m\ll\chi$, by which we obtain

$$\tilde{J}_-=\frac{i\tilde{g}_{om}J_z}{2\left[\chi-i\left(\Omega_m/2-\beta\right)\right]}\tilde{b}=\frac{g_{om}J_z\left(-\gamma+i\beta\right)/\left(2\beta\right)}{2\left[\chi-i\left(\Omega_m/2-\beta\right)\right]}\tilde{b}. \tag{S.24}$$

Substituting Eq. (S.18) and Eq. (S.24) into Eq. (S.23) yields

$$\dot{\tilde{b}}=-\left\{\Gamma_m-\frac{-ig_{om}^2\left(\gamma+i\beta\right)\kappa^2J_z}{8\beta^3\left[\chi-i\left(\Omega_m/2-\beta\right)\right]}\right\}\tilde{b}. \tag{S.25}$$

One finds that the optical modes induce an effective mechanical gain of

$$G=\mathrm{Re}\left\{\frac{-ig_{om}^2\left(\gamma+i\beta\right)\kappa^2J_z}{8\beta^3\left[\chi-i\left(\Omega_m/2-\beta\right)\right]}\right\}=\frac{g_{om}^2\kappa^2\left[\beta\chi+\gamma\left(\Omega_m/2-\beta\right)\right]J_z}{8\beta^3\left[\chi^2+\left(\Omega_m/2-\beta\right)^2\right]}. \tag{S.26}$$

By setting $\Gamma_m=G$, we obtain the threshold of the phonon laser in the regime before the exceptional point

$$P_{\text{threshold}}=\chi\hbar\tilde{\omega}_+a_+^*a_+\approx\chi\hbar\tilde{\omega}_+J_z\approx\frac{8\hbar\Gamma_m\beta^3\chi\left[\chi^2+\left(\Omega_m/2-\beta\right)^2\right]\tilde{\omega}_+}{g_{om}^2\kappa^2\left[\beta\chi+\gamma\left(\Omega_m/2-\beta\right)\right]}, \tag{S.27}$$

where $\tilde{\omega}_+$ is the central frequency of a_+. Here, we have assumed that the phonon laser satisfies the condition of complete inversion such that $N_+ = a_+^* a_+ \approx J_z = a_+^* a_+ - a_-^* a_-$. Considering that $\tilde{\omega}_+ = \omega_0 + \beta \approx \omega_0$, equation (S.27) can be rewritten as

$$P_{\text{threshold}} = \frac{8\hbar\Gamma_m \beta^3 \chi \left[\chi^2 + \left(\Omega_m/2 - \beta \right)^2 \right] \omega_0}{g_{om}^2 \kappa^2 \left[\beta\chi + \gamma \left(\Omega_m/2 - \beta \right) \right]}. \tag{S.28}$$

Let us now take a look on two different limiting cases. First, we consider the situation when the system is far away from the exceptional point such that $2\beta \gg \chi$ and $\kappa \gg \gamma$. In this case, the threshold power given by Eq. (S.28) can be expressed as

$$P_{\text{threshold}} = \frac{8\hbar\Gamma_m \kappa\chi \left[\chi^2 + \left(\Omega_m/2 - \kappa \right)^2 \right] \omega_0}{g_{om}^2}. \tag{S.29}$$

Let us then consider the opposite situation in which the system is in the vicinity of the exceptional point such that $\beta \ll \Omega_m/2,\ \left(\Omega_m\gamma\right)/\left(2\chi\right)$ and $\kappa \approx \gamma$. In this case, equation (S.28) can be simplified to

$$P_{\text{threshold}} = \frac{16\hbar\Gamma_m \beta^3 \chi \left[\chi^2 + \left(\Omega_m/2 \right)^2 \right] \omega_0}{\kappa^3 g_{om}^2\ \Omega_m}. \tag{S.30}$$

It can be seen from Eq. (S.30) that the phonon laser features a very low threshold in the vicinity of the exceptional point, where $\kappa \approx \gamma$ or equivalently $\beta \approx 0$.

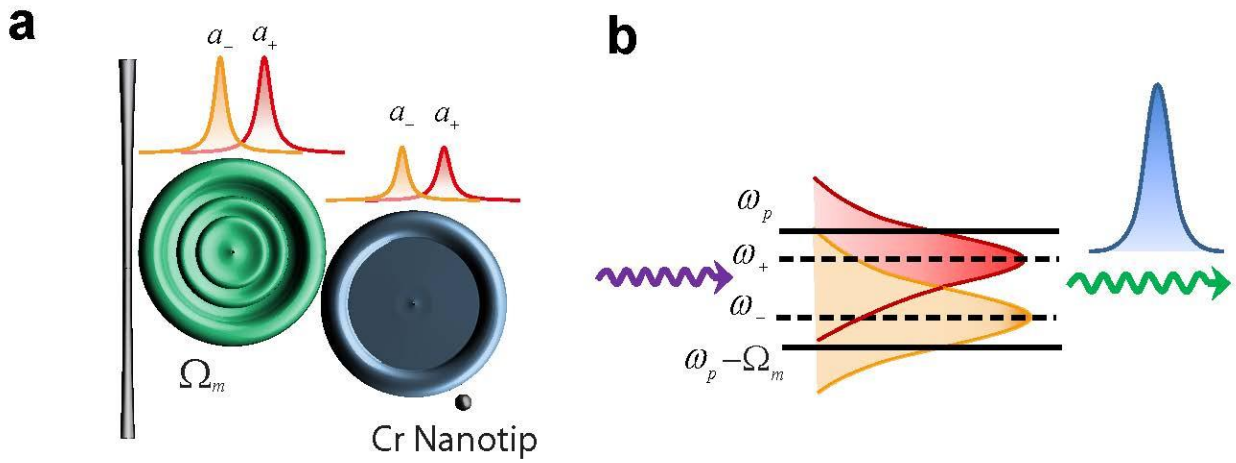

Figure S4. Mechanism of the phonon laser in the regime before the exceptional point. a, Energy distribution of the optical supermodes $a_\pm$ in the two resonators: the optical supermodes $a_\pm$ are almost equally distributed in the left and right resonators. **b,** Distribution of the pump mode and the Stokes mode that stimulate the phonon laser: the pump mode and the Stokes mode are within the frequency bands of the two optical supermodes $a_\pm$.

b. The regime after the exceptional point $\gamma > \kappa$

In the regime after the exceptional point where $\beta = 0,\ \tilde{\beta} \neq 0$, the supermodes of the two-coupled resonators are frequency-degenerate but have different effective damping rates. The high-Q (low-Q) supermode is mainly localized in the microresonator without (with) the Cr-tip. In the vicinity of the exceptional point, the dynamical equations of the system in this regime are then given by

$$\frac{d}{dt}a_- = -\left[\left(\chi - \tilde{\beta}\right) + i\left(\omega_0 - \omega_p\right)\right]a_- - i\frac{\gamma + \tilde{\beta}}{2\tilde{\beta}}g_{\mathrm{om}}a_+ b + \sqrt{2\gamma_{c1}}\tilde{\varepsilon}_-, \tag{S.31}$$

$$\frac{d}{dt}a_+ = -\left[\left(\chi + \tilde{\beta}\right) + i\left(\omega_0 - \omega_p\right)\right]a_+ + i\frac{\gamma + \tilde{\beta}}{2\tilde{\beta}}g_{\mathrm{om}}a_- b^* - \sqrt{2\gamma_{c1}}\tilde{\varepsilon}_+, \tag{S.32}$$

$$\frac{d}{dt}b = -\left(\Gamma_m + i\Omega_m\right)b - ig_{\mathrm{om}}\frac{\left(\gamma + \tilde{\beta}\right)^2}{2\tilde{\beta}^2}a_+^* a_-, \tag{S.33}$$

where $\tilde{\beta}=\sqrt{\gamma^2-\kappa^2}$ and $\tilde{\tilde{\varepsilon}}_{\pm}=-i\kappa\varepsilon\Big/\sqrt{2\gamma^2\pm 2\gamma\tilde{\beta}}$.

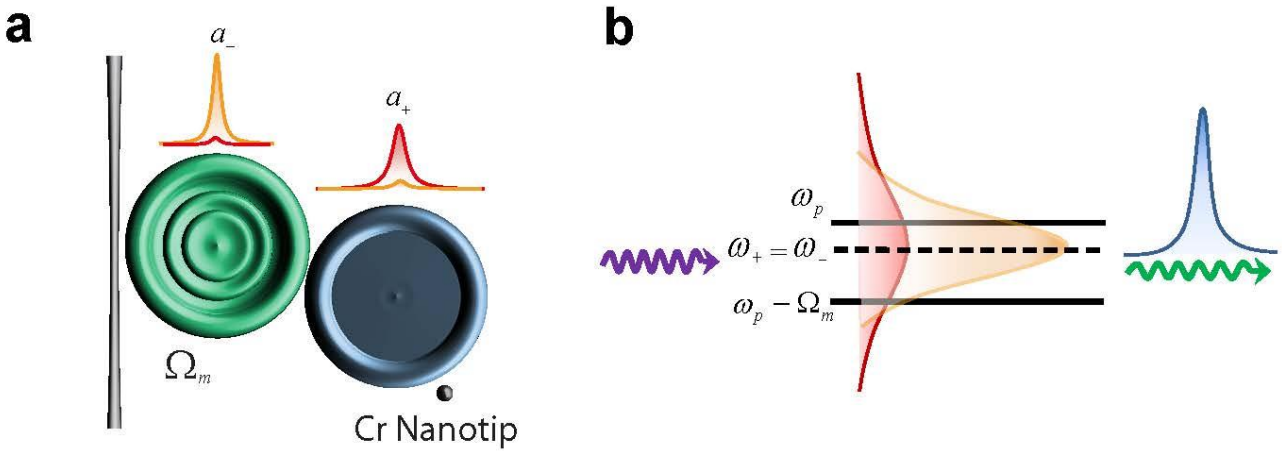

Figure S5. Mechanism of the phonon laser in the regime after the exceptional point. a, Energy distribution of the optical supermodes $a_{\pm}$ in the two resonators: the high-Q optical supermode a_- is mainly distributed in the left resonator supporting the mechanical mode and the low-Q optical supermode a_+ is mainly distributed in the right resonator. **b,** Distribution of the pump mode and the Stokes mode that stimulate the phonon laser: the pump mode and the Stokes mode are mainly distributed in the frequency bands of the high-Q optical supermode a_- and the low-Q optical supermode a_+, which are degenerate.

Similar as before, we redefine the ladder and population inversion operators by the optical modes a_+ and a_- as

$$\bar{J}_-=a_+^*a_-,\qquad \bar{J}_+=a_-^*a_+,\qquad \bar{J}_z=a_-^*a_--a_+^*a_+,$$

and introduce the rotating frame $\tilde{b}=\exp\left(i\Omega_m t\right)b$ and $\tilde{\bar{J}}_-=\exp\left(i\Omega_m t\right)\bar{J}_-$, which leads to

$$\dot{\tilde{\bar{J}}}_-=-2\left(\chi-i\frac{\Omega_m}{2}\right)\tilde{\bar{J}}_-+\frac{ig_{om}\left(\gamma+\tilde{\beta}\right)}{2\tilde{\beta}}\bar{J}_z\tilde{b}, \tag{S.34}$$

$$\dot{\tilde{b}} = -\Gamma_m \tilde{b} - i g_{om} \frac{\left(\gamma + \tilde{\beta}\right)^2}{2\tilde{\beta}^2} \tilde{\bar{J}}_-. \tag{S.35}$$

Adiabatically eliminating the degrees of freedom of the optical modes by setting $\dot{\tilde{J}}_- = 0$ gives

$$\tilde{\bar{J}}_- = \frac{i\left(\gamma + \tilde{\beta}\right) g_{om} \bar{J}_z}{4\tilde{\beta}\left(\chi - i\Omega_m/2\right)} \tilde{b}, \tag{S.36}$$

and substituting this result into Eq. (S.35) yields

$$\dot{\tilde{b}} = -\left[\Gamma_m - \frac{\left(\gamma + \tilde{\beta}\right)^3 g_{om}^2 \bar{J}_z}{8\tilde{\beta}^3\left(\chi - i\Omega_m/2\right)}\right] \tilde{b}. \tag{S.37}$$

Thus, the optical modes induce an effective mechanical gain

$$G = \frac{\left(\gamma + \tilde{\beta}\right)^3 g_{om}^2 \bar{J}_z \chi}{8\tilde{\beta}^3\left[\chi^2 + \left(\Omega_m/2\right)^2\right]}. \tag{S.38}$$

By setting $\Gamma_m = G$, we obtain the threshold of the phonon laser in the regime after the exceptional point,

$$\tilde{P}_{\text{threshold}} = \left(\chi - \tilde{\beta}\right)\hbar\omega_0 \bar{J}_z = \frac{8\hbar\Gamma_m\left(\chi - \tilde{\beta}\right)\tilde{\beta}^3\left[\chi^2 + \left(\Omega_m/2\right)^2\right]\omega_0}{g_{om}^2 \chi\left(\gamma + \tilde{\beta}\right)^3}. \tag{S.39}$$

Similar to the regime before the exceptional point, we want to consider two different limiting cases. First, we treat the situation when the system is far away from the exceptional point such that $\gamma \gg \kappa$. Under these circumstances, the threshold power given by Eq. (S.39) can be expressed as

$$\tilde{P}_{\text{threshold}} = \frac{8\hbar\Gamma_m\left(\chi - \gamma\right)\left[\chi^2 + \left(\Omega_m/2\right)^2\right]\omega_0}{g_{om}^2 \chi}. \tag{S.40}$$

Let us then consider the opposite case in which the system is in the vicinity of the exceptional point such that $\kappa \approx \gamma$. In this case, we have $\chi \gg \tilde{\beta}$, and Eq. (S.39) can be expressed as

$$\tilde{P}_{\text{threshold}} \approx \frac{8\hbar\Gamma_m \tilde{\beta}^3 \left[\chi^2 + \left(\Omega_m/2\right)^2 \right] \omega_0}{g_{om}^2 \gamma^3}, \tag{S.41}$$

which is extremely low in the vicinity of the exceptional point where $\tilde{\beta} \approx 0$.

Employing the system parameters Ω_m=17.38 MHz, $g_{om} = 1.5$ kHz, $\Gamma_m = 40$ kHz, $\gamma_1 = 3.16$ MHz, $\gamma_2 = 13.56$ MHz, we plot the curve of the phonon laser threshold versus the tip-induced loss rate γ_{tip} for

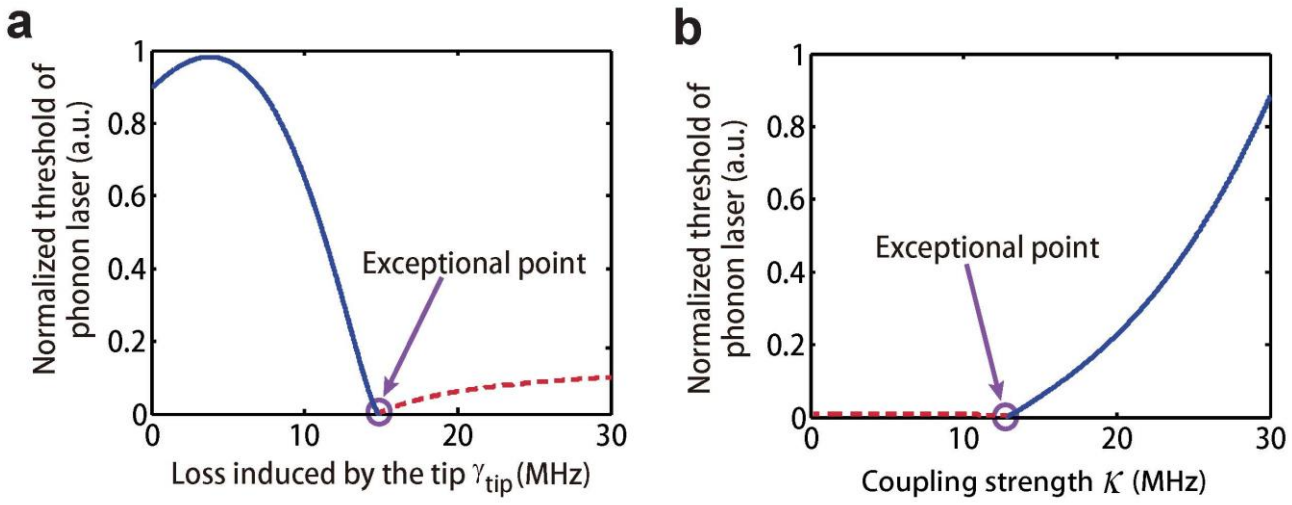

Figure S6. Threshold of the phonon laser $P_{\text{threshold}}$ in the vicinity of the exceptional point. a, $P_{\text{threshold}}$ versus the tip-induced damping rate γ_{tip}. $P_{\text{threshold}}$ first increases with the increase of γ_{tip}, reaches a maximal value, and then decreases with increasing γ_{tip}. Around the exceptional point, there is a sudden drop of $P_{\text{threshold}}$ which represents the transition. **b,** $P_{\text{threshold}}$ versus the coupling strength κ. $P_{\text{threshold}}$ remains to be very small when κ is small and then after the exceptional point, it increases with growing κ. Blue and red curves are obtained using Eqs. (S.30) and (S.41) respectively. The circled points represent the exceptional point where we have $\beta = 0$ and $\tilde{\beta} = 0$ and Eqs. (S.30) and (S.41) become equal.

fixed coupling strength $\kappa = 12.63$ MHz in Fig. S6a and the phonon laser threshold versus the coupling strength κ for fixed $\gamma_{\text{tip}} = 15$ MHz in Fig. S6b. The threshold of the phonon laser is given by Eq. (S.28) and Eq. (S.39). The numerical results in Fig. S6a show a drop of the threshold of the phonon laser in the vicinity of the exceptional point which fits very well with our analysis and the experimental results.

IV. LINEWIDTH OF THE PHONON LASER

a. The regime before the exceptional point $\gamma \le \kappa$

In order to calculate the linewidth of the phonon laser, we have to reconsider the system dynamics by introducing fluctuation terms. In this way, the dynamical equations (S.20)-(S.23) are written as

$$\dot{\tilde{J}}_- = -2\left[\chi - i\left(\Omega_m/2 - \beta\right)\right]\tilde{J}_- + g_{om}\frac{-\gamma + i\beta}{2\beta}J_z\tilde{b} + \xi_-(t), \tag{S.42}$$

$$\dot{\tilde{J}}_+ = -2\left[\chi + i\left(\Omega_m/2 - \beta\right)\right]\tilde{J}_+ + g_{om}\frac{-\gamma - i\beta}{2\beta}\tilde{b}^* J_z + \xi_-^*(t), \tag{S.43}$$

$$\dot{J}_z = -2\chi J_z + g_{om}\frac{\gamma + i\beta}{\beta}\tilde{b}^*\tilde{J}_- + g_{om}\frac{\gamma - i\beta}{\beta}\tilde{b}\tilde{J}_+ + \Lambda + \xi_z(t), \tag{S.44}$$

$$\dot{\tilde{b}} = -\Gamma_m\tilde{b} - ig_{om}\frac{(\gamma + i\beta)^2}{2\beta^2}\tilde{J}_- + \xi_b(t), \tag{S.45}$$

where the noise terms $\xi_-(t), \xi_z(t), \xi_b(t)$ are assumed to be white noises such that [S7]

$$\begin{aligned}
&\left\langle \xi_-(t)\xi_-^\dagger(t')\right\rangle = 2\chi\delta(t-t'), \quad \left\langle \xi_-^\dagger(t)\xi_-(t')\right\rangle = 0, \\
&\left\langle \xi_z(t)\xi_z(t')\right\rangle = 2\chi\delta(t-t'), \\
&\left\langle \xi_b(t)\xi_b^\dagger(t')\right\rangle = 2\Gamma_m(n_{bT}+1)\delta(t-t'), \quad \left\langle \xi_b^\dagger(t)\xi_b(t')\right\rangle = 2\Gamma_m n_{bT}\delta(t-t').
\end{aligned} \tag{S.46}$$

n_{bT} denotes the mean phonon number of the phonon bath in thermal equilibrium. By letting $\dot{\tilde{J}}_- = 0$ and $\dot{\tilde{J}}_+ = 0$ to adiabatically eliminate the degrees of freedom of $\tilde{J}_-$ and $\tilde{J}_+$, we find the following equations for J_z and $\tilde{b}$,

$$\dot{J}_z = -2\chi\left\{1+\frac{g_{om}^2\kappa^2}{4\left[\chi^2+\left(\Omega_m/2-\beta\right)^2\right]\beta^2}n_b\right\}J_z+\Lambda+\tilde{\xi}_z(t), \tag{S.47}$$

$$\dot{\tilde{b}} = -\left\{\Gamma_m-\frac{ig_{om}^2\kappa^2\left(\gamma+i\beta\right)}{8\beta^3\left[\chi-i\left(\Omega_m/2-\beta\right)\right]}J_z\right\}\tilde{b}+\tilde{\xi}_b\left(t\right), \tag{S.48}$$

where $\tilde{\xi}_z(t)$ and $\tilde{\xi}_b(t)$ are effective fluctuation terms which are given by

$$\tilde{\xi}_z(t) = \xi_z(t)+\frac{ig_{om}\left[\left(\beta-i\gamma\right)/\beta\right]}{2\chi-2i\left(\Omega_m/2-\beta\right)}b_{ss}^*\xi_-\left(t\right)+\frac{-ig_{om}\left[\left(\beta+i\gamma\right)/\beta\right]}{2\chi+2i\left(\Omega_m/2-\beta\right)}b_{ss}\xi_-^*(t), \tag{S.49}$$

$$\tilde{\xi}_b(t) = \xi_b\left(t\right)+\frac{-ig_{om}\left(\gamma+i\beta\right)^2}{4\left[\chi-i\left(\Omega_m/2-\beta\right)\right]\beta^2}\xi_-\left(t\right), \tag{S.50}$$

and $b_{ss}=\sqrt{n_{b,ss}}e^{i\phi_{ss}}$ is the stationary value of the phonon field with $\sqrt{n_{b,ss}}$ and ϕ_{ss} respectively being the stationary amplitude and phase of the phonon field. The phonon mode $\tilde{b}$ can be written as

$$\tilde{b} = e^{i\phi_{ss}+i\theta(t)}\left[\sqrt{n_{b,ss}}+\rho\left(t\right)\right], \tag{S.51}$$

where $\theta\left(t\right)$ and $\rho\left(t\right)$ are respectively the phase and amplitude fluctuations of the phonon field. Assuming that the fluctuation terms are small, we have

$$\tilde{b} \approx e^{i\phi_{ss}}\left[1+i\theta\left(t\right)\right]\left[\sqrt{n_{b,ss}}+\rho\left(t\right)\right] \approx \sqrt{n_{b,ss}}e^{i\phi_{ss}}+e^{i\phi_{ss}}\left[\rho\left(t\right)+i\sqrt{n_{b,ss}}\theta\left(t\right)\right]. \tag{S.52}$$

The population inversion J_z can be expressed as the sum of its stationary value and a fluctuation term according to

$$J_z = \frac{8\Gamma_m\beta^3\left[\chi^2+\left(\Omega_m/2-\beta\right)^2\right]}{g_{om}^2\kappa^2\left[\gamma\left(\beta-\Omega_m/2\right)+\chi\beta\right]}+\delta J_z. \tag{S.53}$$

By inserting Eqs. (S.52) and (S.53) into Eq. (S.48), we get

$$\dot{\rho}+i\sqrt{n_{b,ss}}\dot{\theta}=e^{-i\phi_{ss}}\dot{\tilde{b}}=\frac{ig_{om}^{2}\kappa^{2}\left(\gamma+i\beta\right)}{8\beta^{3}\left[\chi-i\left(\Omega_{m}/2-\beta\right)\right]}\sqrt{n_{b,ss}}\delta J_{z}+e^{-i\phi_{ss}}\tilde{\xi}_{b}\left(t\right), \tag{S.54}$$

and therefore

$$\dot{\rho}=\frac{g_{om}^{2}\kappa^{2}\left[\left(\beta-\Omega_{m}/2\right)\gamma-\beta\chi\right]}{8\left[\chi^{2}+\left(\Omega_{m}/2-\beta\right)^{2}\right]\beta^{3}}\sqrt{n_{b,ss}}\delta J_{z}+\xi_{\rho}\left(t\right), \tag{S.55}$$

$$\dot{\theta}=\frac{\left[\chi\gamma+\beta\left(\beta-\Omega_{m}/2\right)\right]g_{om}^{2}\kappa^{2}}{8\left[\chi^{2}+\left(\Omega_{m}/2-\beta\right)^{2}\right]\beta^{3}}\delta J_{z}+\xi_{\theta}\left(t\right), \tag{S.56}$$

in which the fluctuation terms $\xi_{\rho}\left(t\right)$ and $\xi_{\theta}\left(t\right)$ are given by

$$\xi_{\rho}\left(t\right)=\frac{1}{2}\left[e^{-i\phi_{ss}}\tilde{\xi}_{b}\left(t\right)+e^{i\phi_{ss}}\tilde{\xi}_{b}^{\dagger}\left(t\right)\right], \tag{S.57}$$

$$\xi_{\theta}\left(t\right)=\frac{1}{2i\sqrt{n_{b,ss}}}\left[e^{-i\phi_{ss}}\tilde{\xi}_{b}\left(t\right)-e^{i\phi_{ss}}\tilde{\xi}_{b}^{\dagger}\left(t\right)\right]. \tag{S.58}$$

In order to simplify our discussion, we consider the case when $\beta\ll\Omega_{m}/2,\chi,\gamma$, which is fulfilled in the vicinity of the exceptional point. Thus, we can obtain the following approximate equation by substituting Eq. (S.53) into Eq. (S.47)

$$\begin{aligned}\delta\dot{J}_{z}=&-2\chi\left\{1+\frac{g_{om}^{2}\kappa^{2}}{4\left[\chi^{2}+\left(\Omega_{m}/2-\beta\right)^{2}\right]\beta^{2}}\left(n_{b,ss}+2\sqrt{n_{b,ss}}\rho\left(t\right)\right)\right\}\\&\left\{\frac{8\Gamma_{m}\beta^{3}\left[\chi^{2}+\left(\Omega_{m}/2-\beta\right)^{2}\right]}{g_{om}^{2}\kappa^{2}\left(\beta-\Omega_{m}/2\right)\gamma}+\delta J_{z}\right\}+\Lambda+\tilde{\xi}_{z}\left(t\right)\\=&-2\chi\left\{1+\frac{g_{om}^{2}\kappa^{2}}{4\left[\chi^{2}+\left(\Omega_{m}/2-\beta\right)^{2}\right]\beta^{2}}n_{b,ss}\right\}\delta J_{z}-\frac{8\beta\chi\Gamma_{m}}{\gamma\left(\beta-\Omega_{m}/2\right)}\sqrt{n_{b,ss}}\rho\left(t\right)+\tilde{\xi}_{z}\left(t\right).\end{aligned} \tag{S.59}$$

Note that we have used the following equation for the stationary state,

$$\Lambda=\frac{16\chi\Gamma_{m}\left[\chi^{2}+\left(\Omega_{m}/2-\beta\right)^{2}\right]\beta^{3}}{g_{om}^{2}\left(\beta-\Omega_{m}/2\right)\gamma\kappa^{2}}\left[1+\frac{g_{om}^{2}\kappa^{2}}{4\left[\chi^{2}+\left(\Omega_{m}/2-\beta\right)^{2}\right]\beta^{2}}n_{b,ss}\right]. \tag{S.60}$$

Equation (S.59) can be reexpressed as

$$\delta \dot{J}_z = -2\chi\eta\, \delta J_z - \frac{8\beta\chi\Gamma_m}{\gamma\left(\beta-\Omega_m/2\right)}\sqrt{n_{b,ss}}\,\rho(t)+\tilde{\xi}_z(t), \tag{S.61}$$

where

$$\eta = 1+\frac{g_{om}^2\kappa^2}{4\left[\chi^2+\left(\Omega_m/2-\beta\right)^2\right]\beta^2}\, n_{b,ss} = \frac{\Lambda}{\Lambda_{th}}, \tag{S.62}$$

and

$$\Lambda_{th} = \frac{16\chi\Gamma_m\left[\chi^2+\left(\Omega_m/2-\beta\right)^2\right]\beta^3}{g_{om}^2\left(\beta-\Omega_m/2\right)\gamma\kappa^2} \tag{S.63}$$

is the threshold pump for the phonon laser. By combining Eqs. (S.55), (S.56) and (S.61), we obtain the following set of equations for the fluctuation terms

$$\dot{\rho} = \frac{g_{om}^2\kappa^2\left[\left(\beta-\Omega_m/2\right)\gamma-\beta\chi\right]}{8\left[\chi^2+\left(\Omega_m/2-\beta\right)^2\right]\beta^3}\sqrt{n_{b,ss}}\,\delta J_z+\xi_\rho(t), \tag{S.64}$$

$$\dot{\theta} = \frac{g_{om}^2\kappa^2\left[\chi\gamma+\beta\left(\beta-\Omega_m/2\right)\right]}{8\left[\chi^2+\left(\Omega_m/2-\beta\right)^2\right]\beta^3}\,\delta J_z+\xi_\theta(t), \tag{S.65}$$

$$\delta \dot{J}_z = -2\chi\eta\, \delta J_z - \frac{8\beta\chi\Gamma_m}{\gamma\left(\beta-\Omega_m/2\right)}\sqrt{n_{b,ss}}\,\rho(t)+\tilde{\xi}_z(t). \tag{S.66}$$

The linewidth of the phonon laser is related to the fluctuations of the phase $\theta(t)$. Since we have $g_{om} \ll \chi$, we can omit the first term at the right side of Eq. (S.65). While this approximation is necessary for the further calculations, it must be noted, however, that it is not valid in very close vicinity of the EP where $\beta \approx 0$ and therefore the first term in Eq. (S.65) diverges. With this approximation it follows from Eq. (S.65) that

$$\dot{\theta} = \xi_\theta(t), \tag{S.67}$$

which has the formal solution

$$\theta(t)=\int_0^t \xi_\theta(\tau)d\tau, \tag{S.68}$$

and thus

$$\begin{aligned}\left\langle \theta^2(t)\right\rangle &= \int_0^t d\tau' \int_0^t d\tau'' \left\langle \xi_\theta(\tau')\xi_\theta(\tau'')\right\rangle \\ &= \frac{1}{4n_{b,ss}}\int_0^t d\tau' \int_0^t d\tau'' \left[\left\langle \tilde{\xi}_b(\tau')\tilde{\xi}_b^\dagger(\tau'')\right\rangle + \left\langle \tilde{\xi}_b^\dagger(\tau')\tilde{\xi}_b(\tau'')\right\rangle\right].\end{aligned} \tag{S.69}$$

Recapitulating that

$$\tilde{\xi}_b(t)=\xi_b(t)+\frac{-ig_{om}(\gamma+i\beta)^2}{4\left[\chi-i(\Omega_m/2-\beta)\right]\beta^2}\xi_-(t), \tag{S.70}$$

we can write

$$\left\langle \tilde{\xi}_b(\tau')\tilde{\xi}_b^\dagger(\tau'')\right\rangle = 2\Gamma_m\left\{\frac{g_{om}^2\chi\left(\kappa^4/\beta^4\right)}{16\left[\chi^2+(\Omega_m/2-\beta)^2\right]\Gamma_m}+(n_{bT}+1)\right\}\delta(\tau'-\tau''), \tag{S.71}$$

$$\left\langle \tilde{\xi}_b^\dagger(\tau'')\tilde{\xi}_b(\tau')\right\rangle = 2\Gamma_m n_{bT}\delta(\tau'-\tau''). \tag{S.72}$$

Inserting Eqs. (S.71) and (S.72) into Eq. (S.69) results in

$$\left\langle \theta^2(t)\right\rangle = \frac{\Gamma_m}{2n_{b,ss}}\left\{\frac{g_{om}^2\left(\kappa^4/\beta^4\right)\chi}{16\left[\chi^2+(\Omega_m/2-\beta)^2\right]\Gamma_m}+(2n_{bT}+1)\right\}t. \tag{S.73}$$

By substituting Eqs. (S.68) and (S.73) into Eq. (S.51) and noting that $\theta(t)$ is the integral of its corresponding noise, we have [S8]

$$\left\langle \tilde{b}\right\rangle = \sqrt{n_{b,ss}}e^{i\phi_{ss}}\left\langle e^{i\theta(t)}\right\rangle = \sqrt{n_{b,ss}}e^{i\phi_{ss}}e^{-\left\langle\theta^2(t)\right\rangle} = \sqrt{n_{b,ss}}e^{i\phi_{ss}}e^{-\frac{\Gamma_m}{2n_{b,ss}}\left\{\frac{g_{om}^2\left(\kappa^4/\beta^4\right)\chi}{16\left[\chi^2+(\Omega_m/2-\beta)^2\right]\Gamma_m}+(2n_{bT}+1)\right\}t}, \tag{S.74}$$

which means that the linewidth of the phonon laser in this regime can be expressed as

$$\Delta\nu = \frac{\Gamma_m}{2n_{b,ss}}\left\{\frac{g_{om}^2\left(\kappa^4/\beta^4\right)\chi}{16\left[\chi^2+(\Omega_m/2-\beta)^2\right]\Gamma_m}+(2n_{bT}+1)\right\}. \tag{S.75}$$

Additionally, we introduce a phenomenological and power-independent linewidth term $\Delta\nu_0$ in which we pool contributions to the linewidth that are not included in the above model such as those coming from a nonideal population inversion of the medium and from the nonuniformity of the field (as in the case of the optical laser [S9]). Taken together, the linewidth of the phonon laser is then given by

$$\Delta\nu \approx \Delta\nu_0 + \frac{\Gamma_m}{2n_{b,ss}}\left\{\frac{g_{om}^2\left(\kappa^4/\beta^4\right)\chi}{16\left[\chi^2+\left(\Omega_m/2-\beta\right)^2\right]\Gamma_m}+2n_{bT}+1\right\}. \tag{S.76}$$

Using the definition

$$n_{\text{spon}} = \frac{g_{om}^2\left(\kappa^4/\beta^4\right)\chi}{32\left[\chi^2+\left(\Omega_m/2-\beta\right)^2\right]\Gamma_m}, \tag{S.77}$$

we can write the linewidth as follows

$$\Delta\nu \approx \Delta\nu_0 + \frac{\Gamma_m}{2n_{b,ss}}\left(2n_{\text{spon}}+2n_{bT}+1\right). \tag{S.78}$$

With the peak power of the phonon laser P_{peak} being directly proportional to $n_{b,ss}$, this expression shows the same inverse power dependence as in optical laser theory. Analogously to the procedure in optical laser theory [S10], [S11], we have also introduced here the number of spontaneously emitted phonons into the mechanical resonator n_{spon}. In the limit of a perfect match between the frequency difference of the two supermodes and the mechanical resonance frequency, i.e. $2\beta = \Omega_m$, and for equal optical cavity decay rates $\gamma_1 = \gamma_2$, such that $\beta = \kappa$, the expression for n_{spon} simplifies to

$$n_{\text{spon}} = \frac{g_{om}^2}{32\chi\Gamma_m}, \tag{S.79}$$

which is very similar to the already known result from optical laser theory close above the lasing threshold,

$$n_{\mathrm{spon}}^{\mathrm{opt}} = \frac{g^2}{\gamma\Gamma} D_{+,s}, \tag{S.80}$$

in which g represents the coupling between atoms and light, γ the atomic decay rate, Γ the cavity decay rate, and $D_{+,s}$ the saturated occupation of the upper energy level of the two-level system. Using the relation

$$\frac{\gamma\Gamma}{g^2} = D_{+,\mathrm{thr}} - D_{-,\mathrm{thr}}, \tag{S.81}$$

where $D_{+,\mathrm{thr}}$ and $D_{-,\mathrm{thr}}$ are the occupations of the optical supermodes a_+ and a_- at the lasing threshold, the factor n_{spon} can also be expressed by

$$n_{\mathrm{spon}} = \frac{D_{+,s}}{D_{+,\mathrm{thr}} - D_{-,\mathrm{thr}}} \geq 1, \tag{S.82}$$

from which it can be seen that $n_{\mathrm{spon}} \approx 1$ in the case of perfect inversion and close to threshold. Furthermore, we also remark that n_{spon} diverges at an EP occurring in the two-level system, where $D_{+,\mathrm{thr}} = D_{-,\mathrm{thr}}$, and that this divergence can be traced back to the noise term $\xi_-(t)$ in Eq. (S.42), i.e., to the noise in the optical super-modes that provide the gain for the phonon mode. In other words, we can see here how the increased noise in the two-level system directly leads to an increased linewidth in the phonon laser mode.

The difference between the results for our phonon laser given in Eq. (S.79) and for the optical laser given in Eq. (S.80) is a consequence of the different convention for the definitions of β and χ, which causes the factor 32 in the denominator of n_{spon}, as well as of the fact that we have assumed perfect inversion ($D_{+,s} = 1$) for the linewidth derivation above. With the definitions $\beta' \triangleq 2\beta$ and $\chi' \triangleq 2\chi$, Eqs. (S.42)-(S.45) would feature the same structure as the corresponding equations in the optical laser theory [S10], [S11] and we would immediately obtain the result

$$n_{\text{spon}} = \frac{g_{om}^2}{\chi' \Gamma_m}, \tag{S.83}$$

which has exactly the same structure as the corresponding result for the optical laser.

b. The regime after the exceptional point $\gamma > \kappa$

In the regime after the exceptional point, we start from the following dynamical equations including fluctuation terms

$$\dot{\tilde{J}}_- = -2\left(\chi - i\frac{\Omega_m}{2}\right)\tilde{J}_- + \frac{ig_{om}\left(\gamma+\tilde{\beta}\right)}{2\tilde{\beta}}\bar{J}_z\tilde{b} + \xi_-(t), \tag{S.84}$$

$$\dot{\tilde{J}}_+ = -2\left(\chi + i\frac{\Omega_m}{2}\right)\tilde{J}_- - \frac{ig_{om}\left(\gamma+\tilde{\beta}\right)}{2\tilde{\beta}}\bar{J}_z\tilde{b} + \xi_-^*(t), \tag{S.85}$$

$$\dot{\bar{J}}_z = -2\chi\bar{J}_z - \frac{ig_{om}\left(\gamma+\tilde{\beta}\right)}{\beta}\tilde{b}^*\tilde{J}_- + \frac{ig_{om}\left(\gamma+\tilde{\beta}\right)}{\tilde{\beta}}\tilde{b}\tilde{J}_+ + \Lambda + \xi_z(t), \tag{S.86}$$

$$\dot{\tilde{b}} = -\Gamma_m\tilde{b} - ig_{om}\frac{\left(\gamma+\tilde{\beta}\right)^2}{2\tilde{\beta}^2}\tilde{J}_- + \xi_b(t), \tag{S.87}$$

where $\tilde{\beta} = \sqrt{\gamma^2 - \kappa^2}$ and the fluctuation terms $\xi_-(t), \xi_z(t), \xi_b(t)$ satisfy the conditions written in Eq. (S.46). With similar discussions as before, we can obtain the linewidth equation (S.78) with

$$n_{\text{spon}} = \frac{g_{om}^2\left[\left(\gamma+\tilde{\beta}\right)^4/\tilde{\beta}^4\right]\chi}{32\left[\chi^2 + \left(\Omega_m/2\right)^2\right]\Gamma_m}. \tag{S.88}$$

In the vicinity of the exceptional point, where $\tilde{\beta} \approx 0$, Eq. (S.88) simplifies to

$$n_{\text{spon}} \approx \frac{g_{om}^2\kappa^4\chi}{32\tilde{\beta}^4\left[\chi^2 + \left(\Omega_m/2\right)^2\right]\Gamma_m}. \tag{S.89}$$

Using the system parameters Ω_m=17.38 MHz, $g_{om} = 1.5$ kHz, $\Gamma_m = 40$ kHz, $\gamma_1 = 3.16$ MHz, $\gamma_2 = 13.56$

MHz, we plot the normalized linewidth of the phonon laser $\left(\Delta\nu-\Delta\nu_0\right)/P_{\text{peak}}^{-1}$ versus the tip-induced loss rate γ_{tip} for fixed coupling strength $\kappa=12.63$ MHz in Fig. S7a and the normalized linewidth of the phonon laser versus the coupling strength κ for fixed $\gamma_{\text{tip}}=15$ MHz in Fig. S7b. The normalized linewidth of the phonon laser is given by Eq. (S.78) with n_{spon} from Eq. (S.77) in the regime before the exceptional point and from Eq. (S.88) in the regime after the exceptional point, respectively. Both in the regime before the EP and in the regime after the EP, the factor n_{spon} is proportional to β^{-4}, which diverges at the EP and thus leads to an infinite linewidth broadening directly at the EP. We speculate that this problem of the diverging linewidth is due to the approximations necessary to arrive at our analytical results (see above). This divergence is, in fact, already known to occur since the early work by Petermann,

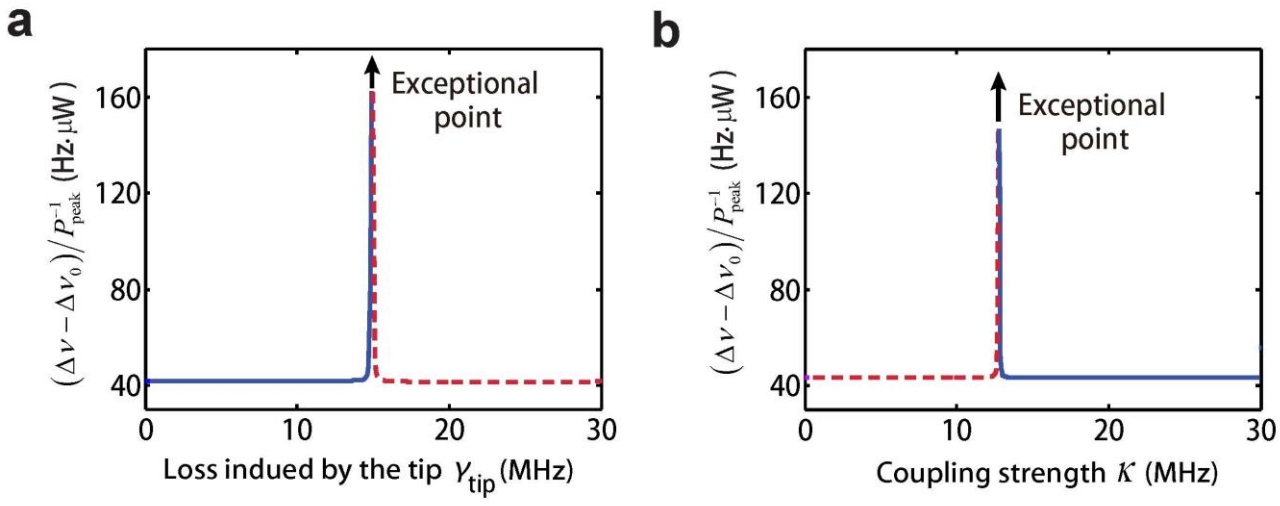

Figure S7. Normalized linewidth of the phonon laser $\left(\Delta\nu-\Delta\nu_0\right)/P_{\text{peak}}^{-1}$ in the vicinity of the exceptional point. a, $\left(\Delta\nu-\Delta\nu_0\right)/P_{\text{peak}}^{-1}$ versus the tip-induced loss rate γ_{tip}. **b,** $\left(\Delta\nu-\Delta\nu_0\right)/P_{\text{peak}}^{-1}$ versus the coupling strength κ. The normalized linewidth of the phonon laser is enhanced in the vicinity of the exceptional point both in (a) and (b).

Siegmann etc. on the linewidth of the optical laser that shows the same divergence. We believe that the linewidth divergence at the EP can be tamed by a more rigorous theoretical approach along the lines of Ref. [S12] in which finite bounds on the enhancement in spontaneous emission at an EP have recently been presented. The challenge will be to merge this new approach with a linewidth calculation as presented above.

V. NONDEGENERATE OPTICAL MODES

In this section, we want to briefly consider the case of non-degenerate (uncoupled) optical cavity resonance frequencies $\omega_1 \neq \omega_2$. Since the two optical modes a_1 and a_2 are coupled to each other, these two modes should be near-resonant. Thus, we can assume that $|\omega_1 - \omega_2| \ll \gamma, \kappa$. Additionally, in order to simplify our discussions, we only consider how this non-ideal case will affect our results in the vicinity of the exceptional point. Thus, we assume that $\beta, \tilde{\beta} \ll |\omega_1 - \omega_2|$. With the above two assumptions, Eqs. (S.4)-(S.6) can be reexpressed as

$$\begin{pmatrix} a_+ \\ a_- \end{pmatrix} = \mathcal{N}^{-1} \begin{pmatrix} \tau_+ & \tau_- \\ 1 & 1 \end{pmatrix}^{-1} \begin{pmatrix} a_1 \\ a_2 \end{pmatrix} = \mathcal{N}^{-1} \begin{pmatrix} \mu & -\lambda \\ -\mu & \lambda \end{pmatrix} \begin{pmatrix} a_1 \\ a_2 \end{pmatrix} \tag{S.90}$$

with complex eigenfrequencies

$$\omega_\pm \approx \omega_p - \omega_0 \pm \sqrt{\gamma |\Delta_-|} - i\chi, \tag{S.91}$$

where $\chi = (\gamma_1 + \gamma_2)/2$, $\gamma = (\gamma_2 - \gamma_1)/2$, $\omega_0 = (\omega_1 + \omega_2)/2$, $\Delta_- = (\omega_2 - \omega_1)/2$, and

$$\tau_\pm \approx \frac{\Delta_- + i\gamma}{\kappa} \pm \frac{\sqrt{\gamma |\Delta_-|}}{\kappa}(1+i) \approx \frac{i\gamma}{\kappa},$$

$$\mu \approx \frac{(1-i)}{4} \sqrt{\frac{\gamma}{|\Delta_-|}},$$

$$\lambda \approx \frac{(1+i)}{4}\sqrt{\frac{\gamma}{|\Delta_-|}},$$

$$\mathcal{N} \approx \frac{1}{2}\sqrt{\frac{\gamma}{|\Delta_-|}}, \tag{S.92}$$

With similar discussions as those in Sec. III and Sec. IV, the threshold and linewidth of the phonon laser can be expressed as

$$P_{\text{threshold}} \approx \frac{16\hbar\Gamma_m\left(\gamma|\Delta_-|\right)^{3/2}\chi\left[\chi^2+\left(\Omega_m/2\right)^2\right]\omega_0}{\kappa^3 g_{om}^2\,\Omega_m}. \tag{S.93}$$

$$\Delta\nu \approx \Delta\nu_0 + \frac{\Gamma_m}{2n_{b,ss}}\left\{\frac{g_{om}^2\kappa^4\chi}{16\gamma^2\Delta_-^2\left[\chi^2+\left(\Omega_m/2-\beta\right)^2\right]\Gamma_m}+2n_{bT}+1\right\}. \tag{S.94}$$

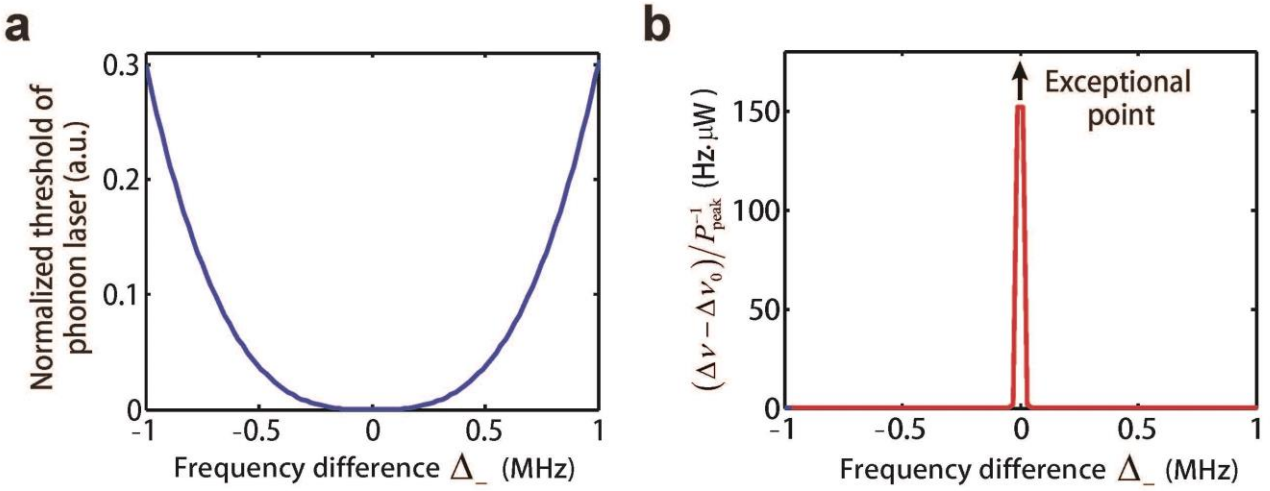

Figure S8. Threshold $P_{\text{threshold}}$ and normalized linewidth of the phonon laser $\left(\Delta\nu-\Delta\nu_0\right)/P_{\text{peak}}^{-1}$ of the phonon laser versus the frequency difference $\Delta_- = \left(\omega_2-\omega_1\right)/2$. a, Normalized threshold of the phonon laser versus Δ_-. **b,** $\left(\Delta\nu-\Delta\nu_0\right)/P_{\text{peak}}^{-1}$ versus Δ_-. The linewidth of the phonon laser decreases very fast in the vicinity of the resonant point $\Delta_- = 0$.

Employing the system parameters Ω_m=17.38 MHz, $g_{om} = 1.5$ kHz, $\Gamma_m = 40$ kHz, $\gamma_1 = 3.16$ MHz, $\gamma_2 = 13.56$ MHz, $\kappa = 12.63$ MHz, $\gamma_{\text{tip}} = 14.85$ MHz, we plot the curves of the phonon laser threshold and the normalized linewidth of the phonon laser $\left(\Delta\nu - \Delta\nu_0\right)\big/ P_{\text{peak}}^{-1}$ versus the frequency difference Δ_- in Fig. S8. It is shown in Fig. S8b that the linewidth of the phonon laser decreases very fast in the vicinity of the resonant point $\Delta_- = 0$.

VI. LINEWIDTH BROADENING OF THE OPTICAL MODES NEAR THE EP

In order to obtain a physical understanding of the mechanism behind the linewidth broadening of the phonon laser, we now take a closer look at the behavior of the optical modes in the vicinity of the EP. Previous work has already demonstrated that the linewidth of an optical laser can be significantly enhanced when the eigenmodes of the system are non-orthogonal [S13], [S14]. In our system, the lasing mode is the mechanical mode while the optical modes are not lasing. As shown below, however, the non-orthogonality of the optical modes in the vicinity of the EP still leads to an enhancement of the effective optical noise strength.

Following a very simple approach, the two coupled optical modes present in our setup can be modeled by a system of beamsplitters [S15], see schematic in Fig. S9a. In this picture the coupling strength between the two optical modes a_1 and a_2 is determined by the reflection and transmission coefficients r and t. Additionally, each of the two optical modes is coupled to a corresponding loss mode (c and d) via beamsplitters with reflection and transmission coefficients r_i and t_i. All reflection and transmission

coefficients satisfy the relation $|r_i|^2 + |t_i|^2 = 1$. One roundtrip in this cavity is then described by the following four-mode unitary scattering matrix,

$$M = \begin{pmatrix} t\,t_1 & r\,t_1 & r_1 & 0 \\ -r\,t_2 & t\,t_2 & 0 & r_2 \\ -t\,r_1 & -r\,r_1 & t_1 & 0 \\ r\,r_2 & -t\,r_2 & 0 & t_2 \end{pmatrix}. \tag{S.95}$$

Since we are only interested in the optical modes a_1 and a_2, we reduce our considerations to the truncated scattering matrix for modes a_1 and a_2,

$$m = \begin{pmatrix} t\,t_1 & r\,t_1 \\ -r\,t_2 & t\,t_2 \end{pmatrix}, \tag{S.96}$$

which is sub-unitary and has non-orthogonal eigenvectors in general. With the help of Eq. (S.96), the input/output relations for the cavity roundtrip can be formulated as follows,

$$a_{1,\mathrm{out}} = t\,t_1\,a_{1,\mathrm{in}} + r\,t_1\,a_{2,\mathrm{in}} + r_1\,a_{1,s}, \tag{S.97}$$

$$a_{2,\mathrm{out}} = t\,t_2\,a_{2,\mathrm{in}} - r\,t_2\,a_{1,\mathrm{in}} + r_2\,a_{2,s}, \tag{S.98}$$

where the spontaneous emission noise contributions $a_{1,s}$ and $a_{2,s}$ are introduced to preserve unitarity. Under the simplifying assumption that a_2 is recoupled onto itself (i.e., $a_{2,\mathrm{out}} = a_{2,\mathrm{in}}$) it is straightforward to calculate the factor by which the noise acting on a_1 is enhanced as compared to the noise present in Eq. (S.97) alone (see Ref. [S15] for further details). This excess noise factor is the well-known Petermann factor given here by the following expression

$$K_1 = 1 + \frac{r^2 t_1^2 r_2^2}{r_1^2\left(1 - t\,t_2\right)^2}. \tag{S.99}$$

Analogously, one can derive the noise enhancement factor for a_2, which is found to be

$$K_2 = 1 + \frac{r^2 r_1^2 t_2^2}{r_2^2 \left(1 - t\, t_1\right)^2}. \tag{S.100}$$

By applying the above formalism to our case, which is described by Eqs. (S.1) and (S.2) with $g_{om} = 0$ and $\Delta \triangleq \omega_p - \omega_0$, we find

$$K_1 = 1 + \frac{\kappa^2 \gamma_2}{\gamma_1 \left(\Delta^2 + \gamma_2^2\right)}, \tag{S.101}$$

$$K_2 = 1 + \frac{\kappa^2 \gamma_1}{\gamma_2 \left(\Delta^2 + \gamma_1^2\right)}. \tag{S.102}$$

Fig. S9b shows the effective optical noise enhancement factor for our system parameters, where one can observe a clear maximum of the curve at the EP, where the eigenmodes of the system are identical. Our calculations thus reveal very clearly that the optical modes continuously increase their noise (i.e. their linewidth) when approaching the EP (without a divergence occurring right at the EP). Since, in turn, the mechanical mode in our phonon laser is driven by these noisy optical supermodes, this increase of the optical noise power is then transferred to the mechanical mode through the optomechanical interaction mechanism. As a result, also the mechanical (phonon) mode features a linewidth broadening when approaching the EP.

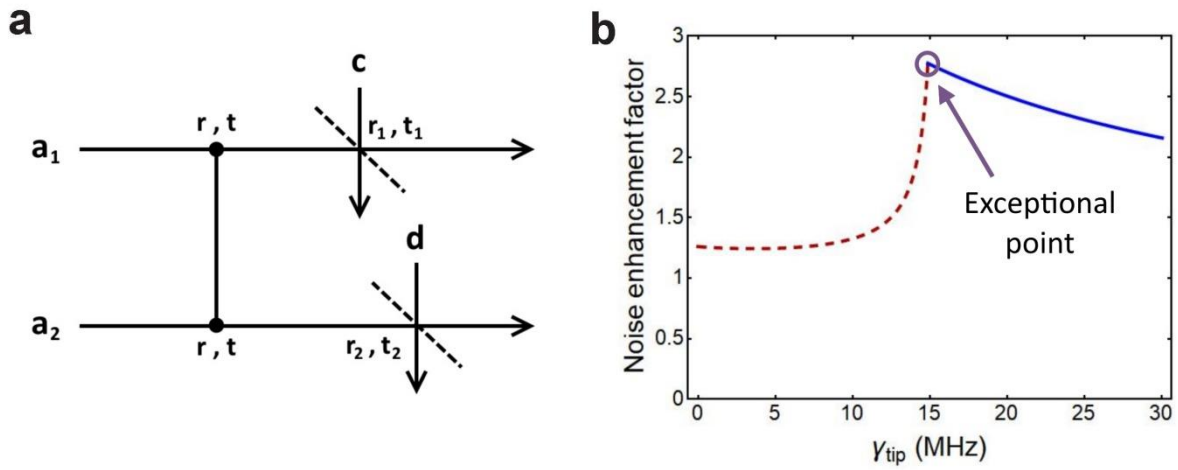

Figure S9. Simplified model for the linewidth broadening due to the non-orthogonality of the optical modes. a, The two optical modes a_1 and a_2 are coupled to two loss modes c and d via mirrors with reflection coefficients r_1 and r_2, and transmission coefficients t_1 and t_2, respectively. Furthermore, we assume a perfect coupling without coupling losses between a_1 and a_2, which is characterized by the reflection and transmission coefficients r and t. **b,** Optical noise enhancement as a function of the additional loss γ_{tip}. The effective optical noise strength features a clear maximum at the EP.

References:

[S1] Grudinin, I. S., Lee, H., Painter, O. & Vahala, K. J. Phonon laser action in a tunable two-level system. *Phys. Rev. Lett.* **104**, 083901 (2010).

[S2] Wang, H., Wang, Z. X., Zhang, J., Ozdemir, S. K., Yang, L. & Liu, Y. X. Phonon amplification in two coupled cavities containing one mechanical resonator. *Phys. Rev. A* **90**, 053814 (2014).

[S3] Mahboob, I., Nishiguchi, K., Fujiwara, A. & Yamaguchi, H. Phonon lasing in an electromechanical resonator. *Phys. Rev. Lett.* **110**, 127202 (2013).

[S4] Jing, H., Ozdemir, S. K., Lü, X.-Y., Zhang, J., Yang, L. & Nori, F. PT-symmetric phonon laser. *Phys. Rev. Lett.* **113**, 053604 (2014).

[S5] Jing, H., Ozdemir, S. K., Geng, Z., Zhang, J., Lü, X.-Y., Peng, B., Yang, L. & Nori, F. Optomechanically-induced transparency in parity-time-symmetric microresonators. *Sci. Rep.* **5**, 9663 (2015).

[S6] Schonleber, D. W., Eisfeld, A. & El-Ganainy, R. Optomechanical interactions in non-Hermitian photonic molecules. *New J. Phys.* **18**, 045014 (2016).

[S7] Walls, D. F. & Milburn, G. J. *Quantum Optics* (Springer, Berlin, 1994).

[S8] Bergli, J., Galperin, Y. M. & Altshuler, B. L. Decoherence in qubits due to low-frequency noise. *New J. Phys.* **11**, 025002 (2009)

[S9] van Exter, M. P., Kuppens, S.J.M. & Woerdman J. P. Theory for the linewidth of a bad-cavity laser. *Phys. Rev. A* **51**, 809-816 (1995).

[S10] Haken, H. Light: Laser Light Dynamics (North-Holland, Amsterdam, 1985), vol. 2.

[S11] Scully, M. & Zubairy, M. Quantum Optics (Cambridge University Press, Cambridge, 1997).

[S12] A. Pick, B. Zhen, O. D. Miller, C. W. Hsu, F. Hernandez, A. W. Rodriguez, M. Soljacic, S. G. Johnson, General theory of spontaneous emission near exceptional points. *Opt. Exp.* **25**, 12325-12348 (2017).

[S13] K. Petermann. Calculated spontaneous emission factor for double-heterostructure injection lasers with gain-induced waveguiding. *IEEE J. Quantum Electron.* **15**, 566 (1979).

[S14] A. E. Siegman. Excess spontaneous emission in non-Hermitian optical systems. *Phys. Rev. A* **39**, 1253 (1989).

[S15] Ph. Grangier and J.-Ph. Poizat. A simple quantum picture for the Petermann excess noise factor. *Eur. Phys. J. D* **1**, 97–104 (1998).